

UNBOUNDED \mathfrak{sl}_3 -LAMINATIONS AROUND PUNCTURES

TSUKASA ISHIBASHI AND SHUNSUKE KANO

ABSTRACT. We continue to study the unbounded \mathfrak{sl}_3 -laminations [IK22], with a focus on their structures at punctures. A key ingredient is their relation to the root data of \mathfrak{sl}_3 . After giving a classification of signed \mathfrak{sl}_3 -webs around a puncture, we describe the tropicalization of the Goncharov–Shen’s Weyl group action in detail. We also clarify the relationship with several other approaches by Shen–Sun–Weng [SSW23] and Fraser–Pylyavskyy [FP21]. Finally, we discuss a formulation of unbounded \mathfrak{g} -laminations for a general semisimple Lie algebra \mathfrak{g} in brief.

CONTENTS

1. Introduction	1
2. Notation	5
3. Unbounded \mathfrak{sl}_3 -laminations	8
4. Structure of unbounded \mathfrak{sl}_3 -laminations around punctures	18
5. Weyl group actions at punctures	21
6. Relation to the work of Shen–Sun–Weng	35
7. Relation to the work of Fraser–Pylyavskyy	39
8. A brief discussion on higher rank generalizations	44
Appendix A. Cluster varieties associated with the pair $(\mathfrak{sl}_3, \Sigma)$	47
Appendix B. Lamination clusters along the mutation sequence representing $r_{p,s}$	54
References	55

1. INTRODUCTION

We continue to study the rational unbounded \mathfrak{sl}_3 -laminations introduced in [IK22], especially focusing on their structure around punctures. Recall from the previous work that we have introduced the space $\mathcal{L}_{\mathfrak{sl}_3}^x(\Sigma, \mathbb{Q})$ of *rational unbounded \mathfrak{sl}_3 -laminations*, which is equipped with the *shear coordinates* $x_\Delta : \mathcal{L}_{\mathfrak{sl}_3}^x(\Sigma, \mathbb{Q}) \xrightarrow{\sim} \mathbb{Q}^{I_{\text{uf}}(\Delta)}$ associated with ideal triangulations Δ of Σ . This space is related to the Douglas–Sun–Kim’s space $\mathcal{L}_{\mathfrak{sl}_3}^a(\Sigma, \mathbb{Q})$ of rational bounded \mathfrak{sl}_3 -laminations [DS20I, Kim21] via the *ensemble map* $p : \mathcal{L}_{\mathfrak{sl}_3}^a(\Sigma, \mathbb{Q}) \rightarrow \mathcal{L}_{\mathfrak{sl}_3}^x(\Sigma, \mathbb{Q})$. The integral points $\mathcal{L}_{\mathfrak{sl}_3}^x(\Sigma, \mathbb{Z})$ are represented by *signed \mathfrak{sl}_3 -webs*, which are \mathfrak{sl}_3 -webs of Kuperberg [Kup96] equipped with a sign on each end incident to a puncture.

In this paper, we study the following structures:

Date: May 8, 2024.

- The *lamination exact sequence*

$$0 \rightarrow (\mathbb{Q}_{\mathbb{Q}}^{\vee})^{\mathbb{M}} \rightarrow \mathcal{L}_{\mathfrak{sl}_3}^a(\Sigma, \mathbb{Q}) \xrightarrow{p} \mathcal{L}_{\mathfrak{sl}_3}^x(\Sigma, \mathbb{Q}) \xrightarrow{\theta} (\mathbb{P}_{\mathbb{Q}}^{\vee})^{\mathbb{M}_o} \rightarrow 0, \quad (1.1)$$

which describes the kernel and the cokernel of the ensemble map. Here \mathbb{Q}^{\vee} and \mathbb{P}^{\vee} denote the coroot and coweight lattices of \mathfrak{sl}_3 , respectively, and the subscript \mathbb{Q} stands for tensoring \mathbb{Q} . The sequence (1.1) leads to a description of the \mathfrak{sl}_3 -laminations around punctures by the root data of \mathfrak{sl}_3 .

- The action of the Weyl group $W(\mathfrak{sl}_3)$ on $\mathcal{L}_{\mathfrak{sl}_3}^x(\Sigma, \mathbb{Q})$ associated with each puncture. This is defined so that it gives the tropicalization of the Weyl group action on the moduli space $\mathcal{X}_{PGL_3, \Sigma}$ of framed PGL_3 -local systems studied by Goncharov–Shen [GS18].

1.1. Lamination exact sequence. The key construction in the sequence (1.1) is the definition of the *tropicalized Casimir map* $\theta = (\theta_p)_{p \in \mathbb{M}_o} : \mathcal{L}_{\mathfrak{sl}_3}^x(\Sigma, \mathbb{Q}) \rightarrow (\mathbb{P}_{\mathbb{Q}}^{\vee})^{\mathbb{M}_o}$, which is introduced as the tropical analogue of the positive map $\Theta_p : \mathcal{X}_{PGL_3, \Sigma} \rightarrow H^{\mathbb{M}_o}$ taking the semisimple part of the monodromy of PGL_3 -local systems around each puncture p . The tropicalized Casimir map assigns a coweight $\theta_p(W)$ to any signed web W , and it turns out that it can be defined as the sum of the local contributions from each end of W incident to p , as illustrated below:



On the ‘dual’ side, the map $(\mathbb{Q}_{\mathbb{Q}}^{\vee})^{\mathbb{M}} \rightarrow \mathcal{L}_{\mathfrak{sl}_3}^a(\Sigma, \mathbb{Q})$ is given by the action at each puncture adding/removing peripheral components.

Here the reader is reminded that in the \mathfrak{sl}_2 -case, the structure of unbounded laminations around a puncture is controlled by a single sign $\{+, -\}$ (or the ‘tag’ in the sense of [FST08]) at each puncture, which corresponds to the root system $\{\alpha, -\alpha\}$ of \mathfrak{sl}_2 .

Recall that we have the *cluster exact sequence* for a general cluster ensemble $(\mathcal{A}, \mathcal{X})$ [FG09] (see Appendix A for a brief review). Here is our first statement, which is obtained by describing (1.1) in terms of the cluster coordinates:

Theorem 1 (Theorem 4.5). *The lamination exact sequence (1.1) coincides with the cluster exact sequence (A.9). In particular, it is equivariant under the action of the cluster modular group $\Gamma_{\mathfrak{sl}_3, \Sigma}$.*

1.2. Weyl group action. The upshot of this paper is the correct definition of the Weyl group action $W(\mathfrak{sl}_3)$ on $\mathcal{L}_{\mathfrak{sl}_3}^x(\Sigma, \mathbb{Q})$. It should be defined so that

- (1) its coordinate expression is the tropical analogue of that of the Goncharov–Shen’s action of $W(\mathfrak{sl}_3)$ on $\mathcal{X}_{PGL_3, \Sigma}$;
- (2) it replaces each end of a given signed web W according to some local rule;

- (3) it makes the tropicalized Casimir map $\theta_p : \mathcal{L}_{\mathfrak{sl}_3}^x(\Sigma, \mathbb{Q}) \rightarrow P_{\mathbb{Q}}^{\vee}$ equivariant, where the action on the target is the usual one on the coweight lattice.

The requirements (2) and (3) uniquely determine the Weyl group action, as follows:

$$r_{p,1} : \begin{array}{ccc} \text{Diagram 1} & \mapsto & \text{Diagram 2} \\ \text{Diagram 3} & \mapsto & \text{Diagram 4} \end{array} \quad (1.2)$$

The diagrams in (1.2) are as follows:
 - Diagram 1: A dashed circle containing a red vertical line with an upward arrow and a '+' sign to its left.
 - Diagram 2: A dashed circle containing a red vertical line with an upward arrow and a '+' sign to its left.
 - Diagram 3: A dashed circle containing a red vertical line with an upward arrow and a '-' sign to its left.
 - Diagram 4: A dashed circle containing a red vertical line with an upward arrow and a '+' sign to its right, and a red circular arrow (loop) with a '-' sign to its left.

$$r_{p,2} : \begin{array}{ccc} \text{Diagram 5} & \mapsto & \text{Diagram 6} \\ \text{Diagram 7} & \mapsto & \text{Diagram 8} \end{array} \quad (1.3)$$

The diagrams in (1.3) are as follows:
 - Diagram 5: A dashed circle containing a red vertical line with an upward arrow and a '+' sign to its left.
 - Diagram 6: A dashed circle containing a red vertical line with an upward arrow and a '+' sign to its right, and a red circular arrow (loop) with a '-' sign to its left.
 - Diagram 7: A dashed circle containing a red vertical line with an upward arrow and a '-' sign to its left.
 - Diagram 8: A dashed circle containing a red vertical line with an upward arrow and a '-' sign to its left.

However, it turns out that such an action produces *resolvable pairs* of ends at a puncture (the right-most one in (3.3)) that we have prohibited in the previous paper [IK22]. The actual problem is the following: as its name suggests, such a resolvable pair can be “resolved” into an arc away from puncture without changing its shear coordinates (Definition 5.1 Step 0). However, such an operation in turn produces possible intersections with other parts of the web, which are also prohibited. In view of the relation to the skein algebra [IK22, Section 5], it would be natural to further “resolve” these additional intersections using a kind of skein relation.

These observations lead us to a detailed study of resolution operations of the resolvable pairs and the additional intersections, without affecting the shear coordinates (Section 5). Such an operation would be of independent interest, in view of the expectation that the signed webs should parametrize a basis of a certain skein algebra and that the equivalence relations among them pick up the “highest terms” in some sense from appropriate skein relations.

Eventually, we can resolve all such prohibited things to get a usual signed web. Then we obtain:

Theorem 2 (Proposition 5.9 and Theorem 5.11). *We have a well-defined action of $W(\mathfrak{sl}_3)^{\mathbb{M}_0}$ on $\mathcal{L}_{\mathfrak{sl}_3}^x(\Sigma, \mathbb{Q})$ specified by the local rules in (1.2) and (1.3). Moreover, it coincides with the tropicalization of the Goncharov–Shen’s action [GS18].*

1.3. Relation to the work of Shen–Sun–Weng. In their recent work [SSW23], Shen–Sun–Weng introduced a pairing between ‘ \mathcal{A} -webs’ and ‘ \mathcal{X} -webs’, which is expected to provide a topological construction of a duality pairing as described in [FG09, Conjecture 4.3].

In our terminology, their \mathcal{A} -webs correspond to the bounded integral \mathfrak{sl}_3 -laminations without negative peripheral components. They also conjectured that the \mathcal{X} -webs corresponds to a subspace $\mathcal{P}_{PGL_3, \Sigma}^+(\mathbb{Z}^T) \subset \mathcal{P}_{PGL_3, \Sigma}(\mathbb{Z}^T)$ cut out by certain conditions [SSW23, Conjecture 4.10], where the latter denotes the set of integral tropical points of the Goncharov–Shen’s moduli space $\mathcal{P}_{PGL_3, \Sigma}$ [GS19]. We construct a bijection between the space $\mathcal{W}_{\Sigma}^{\mathcal{X}}$ of their \mathcal{X} -webs and a certain subspace $\mathcal{L}_{\mathfrak{sl}_3}^p(\Sigma, \mathbb{Z})_0$ of the integral \mathcal{P} -laminations [IK22, Section 4], and give a proof of their conjecture based on the result [IK22, Theorem 4.11] in our previous work (together with Proposition 4.4).

Since the definition of \mathcal{X} -webs involves no signs and pinnings, this relation would serve as a simpler understanding of the subset $\mathcal{L}_{\mathfrak{sl}_3}^p(\Sigma, \mathbb{Z})_0$. On the other hand, we certainly need signs (and pinnings) to describe the entire space $\mathcal{P}_{PGL_3, \Sigma}(\mathbb{Z}^T)$. As the duality pairing should be equivariant under the Weyl group actions, our study on the Weyl group action will be a key ingredient to complete their construction to an entire pairing $\mathcal{A}_{PGL_3, \Sigma}(\mathbb{Z}^T) \times \mathcal{P}_{PGL_3, \Sigma}(\mathbb{Z}^T) \rightarrow \frac{1}{3}\mathbb{Z}$.

1.4. Relation to the work of Fraser–Pylyavskyy. In the case where Σ has no punctures, we have seen that the unbounded integral \mathfrak{sl}_3 -laminations give a basis for the (upper) cluster algebra related to the pair $(\mathfrak{sl}_3, \Sigma)$ [IK22, Corollary 5.7], which is also the same as the function ring $\mathcal{O}(\mathcal{A}_{SL_3, \Sigma}^{\times})$ of (a certain generic part of) the moduli space of decorated SL_3 -local systems [FG06a, IOS23]. It is still natural to expect that our unbounded integral \mathfrak{sl}_3 -laminations give a basis for one of these algebras in the presence of punctures.

Fraser–Pylyavskyy [FP21] gave an approach in this direction by representing certain (rational) functions on $\mathcal{A}_{SL_k, \Sigma}$ by *pseudo-tagged diagrams*, which are webs equipped with certain decoration data at ends. In Section 7, we give a comparison between our signed webs and the pseudo-tagged diagrams for $k = 3$.

While the Fraser–Pylyavskyy’s pseudo-tagged diagrams directly encodes the representation-theoretic decoration data of SL_3 -local systems (*i.e.*, a flat section of the associated SL_3/U -bundle), our data of signs at punctures would be thought of as a tropical analogue of the *framings* of convex \mathbb{RP}^2 -structures [FG07b].

1.5. Higher rank generalizations. Finally, we discuss in brief higher rank generalizations, namely the unbounded \mathfrak{g} -laminations associated with any semisimple Lie algebra \mathfrak{g} . We propose to use the approach of Murakami–Ohtsuki–Yamada [MOY98] and Cautis–Kamnitzer–Morrison [CKM14] as a model of \mathfrak{g} -webs, and to define a rational unbounded \mathfrak{g} -lamination to be a certain equivalence class of the *signed \mathfrak{g} -webs* with rational weights. Here, the signed \mathfrak{g} -webs are equipped with signs $\{+, -\}$ on their ends just as in the \mathfrak{sl}_3 -case, and we do not expect any further decoration data needed since the colors by fundamental weights of \mathfrak{g} and these signs are sufficient to exhaust the coweight lattice via the tropicalized Casimir map θ_p (Figure 20). We also discuss their shear coordinates.

Organization of the paper. Our notations on the marked surfaces and Lie theory are summarized in Section 2. In Section 3, we recall the definition of unbounded \mathfrak{sl}_3 -laminations and their shear coordinates.

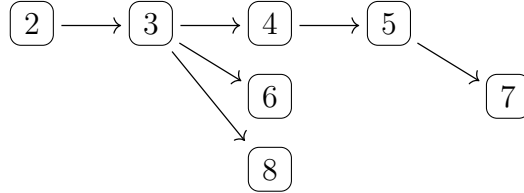
Section 4.1 gives a classification of unbounded \mathfrak{sl}_3 -laminations around a puncture. In Section 4.2, we describe our constructions in the shear coordinates, and relate them to the cluster exact sequence coming from the structure of cluster ensemble [FG09].

Section 5 is the most involved part, which describes the Weyl group action on the unbounded \mathfrak{sl}_3 -laminations. Some of the technical statements are proved in Section 5.3.

In Section 6, we give a proof of the Shen–Sun–Weng’s conjecture by using the fact that our tropicalized Casimir map θ_p is indeed the tropicalization of the positive map Θ_p on the moduli space $\mathcal{P}_{PGL_3, \Sigma}$.

In Section 7, we investigate several relations to the work of Fraser–Pylyavskyy. We relate our signed webs with their ‘pseudo-tagged diagrams’. Finally in Section 8, we briefly discuss the higher rank generalizations.

The following diagram shows the relationships among Sections 2–8.



Acknowledgements. The authors are grateful to Wataru Yuasa and Zhe Sun for valuable discussions on the \mathfrak{sl}_3 -skein relations at punctures. T. I. is partially supported by JSPS KAKENHI (20K22304). S. K. is partially supported by scientific research support of Research Alliance Center for Mathematical Sciences, Tohoku University.

2. NOTATION

2.1. Marked surfaces and their triangulations. A marked surface (Σ, \mathbb{M}) is a compact oriented surface Σ together with a fixed non-empty finite set $\mathbb{M} \subset \Sigma$ of *marked points*. When the choice of \mathbb{M} is clear from the context, we simply denote a marked surface by Σ . A marked point is called a *puncture* if it lies in the interior of Σ , and a *special point* otherwise. Let \mathbb{M}_o (resp. \mathbb{M}_∂) denote the set of punctures (resp. special points), so that $\mathbb{M} = \mathbb{M}_o \sqcup \mathbb{M}_\partial$. Let $\Sigma^* := \Sigma \setminus \mathbb{M}_o$. We always assume the following conditions:

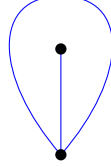
- (S1) Each boundary component (if exists) has at least one marked point.
- (S2) $-2\chi(\Sigma^*) + |\mathbb{M}_\partial| > 0$.
- (S3) (Σ, \mathbb{M}) is not a once-punctured disk with a single special point on the boundary.

We call a connected component of the punctured boundary $\partial^*\Sigma := \partial\Sigma \setminus \mathbb{M}_\partial$ a *boundary interval*. The set of boundary intervals is denoted by \mathbb{B} .

Unless otherwise stated, an *isotopy* in a marked surface (Σ, \mathbb{M}) means an ambient isotopy in Σ relative to \mathbb{M} , which preserves each boundary interval setwisely. An *ideal*

arc in (Σ, \mathbb{M}) is an immersed arc in Σ with endpoints in \mathbb{M} which has no self-intersection except possibly for its endpoints, and is not isotopic to one point.

An *ideal triangulation* is a triangulation Δ of Σ whose set of 0-cells (vertices) coincides with \mathbb{M} . The conditions (S1) and (S2) ensure the existence of such an ideal triangulation, and the positive integer in (S2) gives the number of 2-cells (triangles). In this paper, we always consider an ideal triangulation without *self-folded triangles* of the form



whose existence is ensured by the condition (S3). See, for instance, [FST08, Lemma 2.13]. For an ideal triangulation Δ , denote the set of edges (resp. interior edges, triangles) of Δ by $e(\Delta)$ (resp. $e_{\text{int}}(\Delta)$, $t(\Delta)$). Since the boundary intervals belong to any ideal triangulation, $e(\Delta) = e_{\text{int}}(\Delta) \sqcup \mathbb{B}$. By a computation on the Euler characteristics, we get

$$\begin{aligned} |e(\Delta)| &= -3\chi(\Sigma^*) + 2|\mathbb{M}_\partial|, & |e_{\text{int}}(\Delta)| &= -3\chi(\Sigma^*) + |\mathbb{M}_\partial|, \\ |t(\Delta)| &= -2\chi(\Sigma^*) + |\mathbb{M}_\partial|. \end{aligned}$$

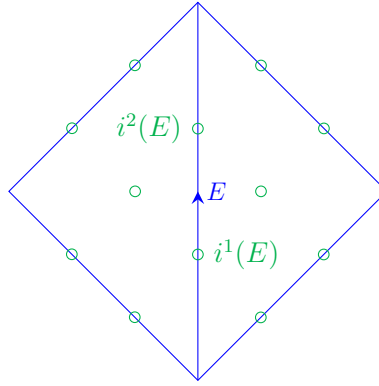


FIGURE 1. The set $I(\Delta)$ of distinguished points.

To indicate the \mathfrak{sl}_3 -structure, it is useful to equip Δ with two distinguished points on the interior of each edge and one point in the interior of each triangle, as shown in Figure 1. The set of such points is denoted by $I(\Delta) = I_{\mathfrak{sl}_3}(\Delta)$. This set will give the vertex set of the quiver Q^Δ associated with Δ : see Appendix A.2. Let $I^{\text{edge}}(\Delta)$ (resp. $I^{\text{tri}}(\Delta)$) denote the set of points on the interiors of edges (resp. triangles) so that $I(\Delta) = I^{\text{edge}}(\Delta) \sqcup I^{\text{tri}}(\Delta)$, where we have a canonical bijection

$$t(\Delta) \xrightarrow{\sim} I^{\text{tri}}(\Delta), \quad T \mapsto i(T).$$

When we need to label the two vertices on an edge $E \in e(\Delta)$, we endow it with an orientation. Then let $i^1(E) \in I(\Delta)$ (resp. $i^2(E) \in I(\Delta)$) denote the vertex closer to the

initial (resp. terminal) endpoint of E . Let $I(\Delta)_f \subset I^{\text{edge}}(\Delta)$ (“frozen”) be the subset consisting of the points on the boundary, and let $I(\Delta)_{\text{uf}} := I(\Delta) \setminus I(\Delta)_f$ (“unfrozen”). The numbers

$$|I(\Delta)| = 2|e(\Delta)| + |t(\Delta)| = -8\chi(\Sigma^*) + 5|\mathbb{M}_{\partial}|$$

and

$$|I(\Delta)_{\text{uf}}| = 2|e_{\text{int}}(\Delta)| + |t(\Delta)| = -8\chi(\Sigma^*) + 3|\mathbb{M}_{\partial}|$$

will give the dimensions of the PL manifolds $\mathcal{L}_{\mathfrak{sl}_3}^a(\Sigma, \mathbb{R})$ and $\mathcal{L}_{\mathfrak{sl}_3}^x(\Sigma, \mathbb{R})$ respectively, which we will study in this paper.

2.2. Notation from Lie theory. For a complex semisimple finite-dimensional Lie algebra \mathfrak{g} , choose a Cartan subalgebra \mathfrak{h} and a set of simple roots. Let S be the vertex set of the associated Dynkin diagram. Then we have the following lattices:

- $Q = \bigoplus_{s \in S} \mathbb{Z}\alpha_s \subset \mathfrak{h}^*$ (root lattice),
- $P = \bigoplus_{s \in S} \mathbb{Z}\varpi_s \subset \mathfrak{h}^*$ (weight lattice),
- $Q^\vee = \bigoplus_{s \in S} \mathbb{Z}\alpha_s^\vee \subset \mathfrak{h}$ (coroot lattice),
- $P^\vee = \bigoplus_{s \in S} \mathbb{Z}\varpi_s^\vee \subset \mathfrak{h}$ (coweight lattice).

Here α_s , ϖ_s , α_s^\vee , ϖ_s^\vee are called the s -th simple root, fundamental weight, simple coroot, fundamental coweight, respectively for $s \in S$. We have the relations

$$\alpha_t = \sum_s C_{st} \varpi_s \quad \text{and} \quad \alpha_t^\vee = \sum_s C_{ts} \varpi_s^\vee,$$

where $C(\mathfrak{g}) = (C_{st})_{s,t \in S}$ is the Cartan matrix of \mathfrak{g} . The relations among the lattices above are summarized as follows:

$$Q^\vee = \text{Hom}(P, \mathbb{Z}), \quad P^\vee = \text{Hom}(Q, \mathbb{Z}), \quad Q \subset P, \quad Q^\vee \subset P^\vee.$$

Here the inclusions are of index $\det C(\mathfrak{g})$. For a lattice L , let $L_{\mathbb{Q}} := L \otimes_{\mathbb{Z}} \mathbb{Q}$ denote the associated \mathbb{Q} -vector space.

Let G (resp. G') be the simply-connected (resp. adjoint) algebraic group with the Lie algebra \mathfrak{g} . Let $H \subset G$ be a Cartan subgroup, and $H' \subset G'$ be its image under the canonical projection. Then the lattices above are interpreted as (co)character lattices:

$$\begin{aligned} P &= X^*(H), & Q^\vee &= X_*(H), \\ Q &= X^*(H'), & P^\vee &= X_*(H'). \end{aligned}$$

Here $X^*(T) := \text{Hom}(T, \mathbb{G}_m)$ and $X_*(T) := \text{Hom}(\mathbb{G}_m, T)$ for a split algebraic torus T . The cocharacter lattice $X_*(T)$ can be viewed as the tropical analogue of T (cf. [FG09]).

The \mathfrak{sl}_3 -case. The groups are $G = SL_3$ and $G' = PGL_3$. The standard choice of Cartan subgroup is $H := \{\text{diag}(x, y, z) \mid xyz = 1\} \subset SL_3$, leading to $P = \mathbb{Z}^3/\mathbb{Z}(1, 1, 1)$ and $Q^\vee = \{(a, b, c) \mid a + b + c = 0\} \subset \mathbb{Z}^3$.

- Simple positive roots:

$$\alpha_1 = \text{diag}(1, -1, 0), \quad \alpha_2 = \text{diag}(0, 1, -1).$$

- Fundamental weights:

$$\varpi_1 = \text{diag}(2/3, -1/3, -1/3), \quad \varpi_2 = \text{diag}(1/3, 1/3, -2/3).$$

- The Cartan matrix:

$$C(\mathfrak{sl}_3) = \begin{pmatrix} 2 & -1 \\ -1 & 2 \end{pmatrix}.$$

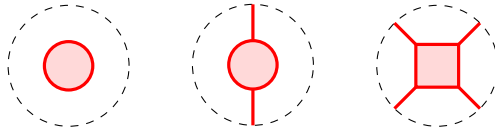
3. UNBOUNDED \mathfrak{sl}_3 -LAMINATIONS

3.1. Definition. Let us briefly recall the definition of the rational unbounded \mathfrak{sl}_3 -laminations from [IK22, Section 2].

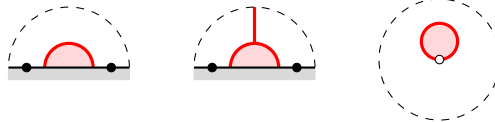
An \mathfrak{sl}_3 -web (or simply a *web*) on a marked surface Σ is an immersed oriented uni-trivalent graph W on Σ such that each univalent vertex lies in $\mathbb{M}_\circ \cup \partial^*\Sigma$, and the other part is embedded into $\text{int } \Sigma^*$. Here, the orientation is given so that each trivalent vertex is either a *sink* or a *source*, respectively:



We also allow oriented loop components. A web is said to be *non-elliptic* if it has none of the following *elliptic faces*:



(3.1)



(3.2)

A web is said to be *bounded* if none of its univalent vertices lie in \mathbb{M}_\circ .

A *signed web* is a web on Σ together with a sign (+ or −) assigned to each end incident to a puncture. The following patterns (and their orientation-reversals) of signed ends are

called *bad ends*:

$$(3.3)$$

Here $\epsilon \in \{+, -\}$. The pair of ends of the first type is called the *resolvable pair*. A signed web is said to be *admissible* if it has no bad ends. Unless otherwise stated, we always assume that the signed webs are admissible (until Section 5). A bounded web is naturally regarded as a signed web, since we do not need to specify any signs.

Elementary moves of signed webs. We are going to introduce several elementary moves for signed webs. The first two are defined for a web without signs.

(E1) Loop parallel-move (a. k. a. *flip move* [FS20] or *global parallel move* [DS20I]):

$$(3.4)$$

(E2) Boundary H-move:

$$(3.5)$$

Similarly for the opposite orientation. We call the face in the left-hand side a *boundary H-face*.

(E3) Puncture H-moves:

$$(3.6)$$

for $\epsilon \in \{+, -\}$, and

$$(3.7)$$


Similarly for the opposite orientation. We call the face in the left-hand side of (3.6) a *puncture H-face*.

The moves (E2) and the first one in (E3) lead to the parallel-moves for the arcs. See [IK22, Lemma 2.4].

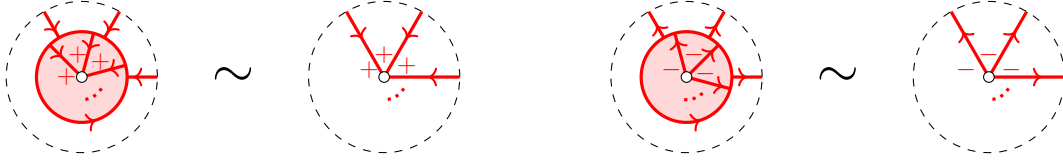
Also note that we can always transform any signed web to a signed web without boundary H-faces (resp. puncture H-faces) by applying (E2) and (E3), respectively. Slightly generalizing the terminology in [FS20], such a signed web is said to be *boundary-reduced*

(resp. *puncture-reduced*). It is said to be *reduced* if it is both boundary- and puncture-reduced.

(E4) Peripheral move: removing or creating a peripheral component:


(3.8)

Moreover, we have the moves

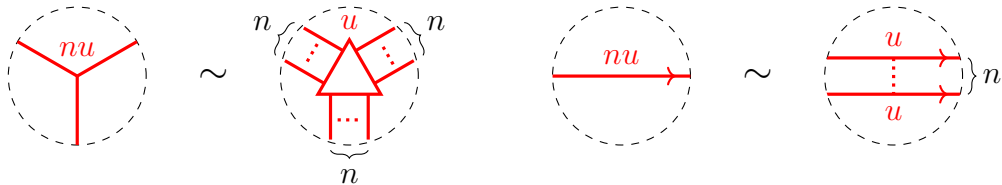


Similarly for the opposite orientation.

We will consider the equivalence relation on signed webs generated by isotopies of marked surfaces and the elementary moves (E1)–(E4). Observe that the moves (E1)–(E4) preserves the admissibility. On the other hand, a non-elliptic signed web may be equivalent to an elliptic web. See [IK22, Example 2.5] for an example.

Definition 3.1 (rational unbounded \mathfrak{sl}_3 -laminations). A *rational unbounded \mathfrak{sl}_3 -lamination* (or a rational \mathfrak{sl}_3 - \mathcal{X} -lamination) on Σ is an admissible, non-elliptic signed \mathfrak{sl}_3 -web W on Σ equipped with a positive rational number (called the *weight*) on each component, which is considered modulo the equivalence relation generated by isotopies and the following operations:

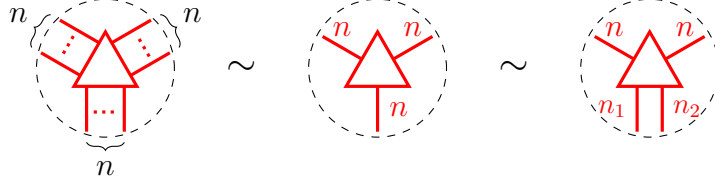
- (1) Elementary moves (E1)–(E4) for the underlying signed webs. Here the corresponding components are assumed to have the same weights.
- (2) Combine a pair of isotopic loops with the same orientation with weights u and v into a single loop with the weight $u + v$. Similarly combine a pair of isotopic oriented arcs with the same orientation (and with the same signs if some of their ends are incident to punctures) into a single one by adding their weights.
- (3) For an integer $n \in \mathbb{Z}_{>0}$ and a rational number $u \in \mathbb{Q}_{>0}$, replace a component with weight nu with its n -cabling with weight u , which locally looks like



For a loop or arc component, it is just the $n - 1$ times applications of the operation (2). One can also verify that the cabling operation is associative in the sense that the n -cabling followed by the m -cabling agrees with the nm -cabling.

Let $\mathcal{L}_{\mathfrak{sl}_3}^x(\Sigma, \mathbb{Q})$ denote the set of equivalence classes of the rational unbounded \mathfrak{sl}_3 -laminations on Σ . We have a natural $\mathbb{Q}_{>0}$ -action on $\mathcal{L}_{\mathfrak{sl}_3}^x(\Sigma, \mathbb{Q})$ that simultaneously rescales the weights. A rational unbounded \mathfrak{sl}_3 -lamination is said to be *integral* if all the weights are integers. The subset of integral unbounded \mathfrak{sl}_3 -laminations is denoted by $\mathcal{L}_{\mathfrak{sl}_3}^x(\Sigma, \mathbb{Z})$.

Notation 3.2. In view of the equivalence relation (4), we will occasionally use the following equivalent notations for honeycombs:



with $n_1 + n_2 = n$. We may also split an edge of weight n with k edges of weight n_1, \dots, n_k with $n_1 + \dots + n_k = n$.

Definition 3.3 (Dynkin involution). The *Dynkin involution* is the involutive automorphism

$$* : \mathcal{L}_{\mathfrak{sl}_3}^x(\Sigma, \mathbb{Q}) \rightarrow \mathcal{L}_{\mathfrak{sl}_3}^x(\Sigma, \mathbb{Q}), \quad \widehat{L} \mapsto \widehat{L}^*,$$

where \widehat{L}^* is obtained from \widehat{L} by reversing the orientation of every components of the underlying web, and keeping the signs at punctures intact. Since all the elementary moves (E1)–(E4) are equivariant under the orientation-reversion, this indeed defines an automorphism on $\mathcal{L}_{\mathfrak{sl}_3}^x(\Sigma, \mathbb{Q})$.

Bounded laminations and the ensemble map.

Definition 3.4 (rational bounded \mathfrak{sl}_3 -laminations). A *rational bounded \mathfrak{sl}_3 -lamination* (or a *rational \mathfrak{sl}_3 - \mathcal{A} -lamination*) on Σ is a bounded non-elliptic \mathfrak{sl}_3 -web W on Σ equipped with a rational number (called the *weight*) on each component such that the weight on a non-peripheral component is positive. It is considered modulo the equivalence relation generated by isotopies and the operations (2)–(4) in Definition 3.1.

Let $\mathcal{L}_{\mathfrak{sl}_3}^a(\Sigma, \mathbb{Q})$ denote the space of rational bounded \mathfrak{sl}_3 -laminations. We have a natural $\mathbb{Q}_{>0}$ -action on $\mathcal{L}_{\mathfrak{sl}_3}^a(\Sigma, \mathbb{Q})$ that simultaneously rescales the weights. A rational bounded \mathfrak{sl}_3 -lamination is said to be *integral* if all the weights are integers. The subset of integral bounded \mathfrak{sl}_3 -laminations is denoted by $\mathcal{L}_{\mathfrak{sl}_3}^a(\Sigma, \mathbb{Z})$. For the relation to the works of Douglas–Sun [DS20I, DS20II] and Kim [Kim21], see [IK22, Remark 2.10].

By forgetting the peripheral components, we get the *geometric ensemble map*

$$p : \mathcal{L}_{\mathfrak{sl}_3}^a(\Sigma, \mathbb{Q}) \rightarrow \mathcal{L}_{\mathfrak{sl}_3}^x(\Sigma, \mathbb{Q}). \quad (3.9)$$

In the next subsection, we will describe the ‘kernel’ and the ‘cokernel’ of the geometric ensemble map p .

3.2. Lamination exact sequence.

3.2.1. *The tropicalized Casimir map on $\mathcal{L}_{\mathfrak{sl}_3}^x(\Sigma, \mathbb{Q})$.* For each puncture $p \in \mathbb{M}_o$, we define a function

$$\theta_p : \mathcal{L}_{\mathfrak{sl}_3}^x(\Sigma, \mathbb{Q}) \rightarrow \mathbb{P}_{\mathbb{Q}}^{\vee}$$

which we call the *tropicalized Casimir map* associated with p , as follows. For a rational \mathfrak{sl}_3 -lamination $\widehat{L} \in \mathcal{L}_{\mathfrak{sl}_3}^x(\Sigma, \mathbb{Q})$ with a support W , the coweight $\theta_p(\widehat{L}) \in \mathbb{P}_{\mathbb{Q}}^{\vee}$ is defined to be the sum of the contributions from each end of the web W incident to p , given as in Figure 2. Then it is clearly invariant under the equivalence relation in Definition 3.1.

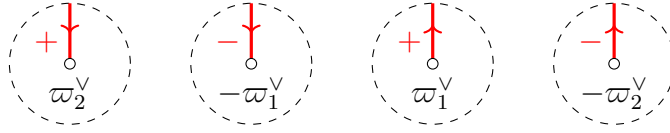


FIGURE 2. Contribution to $\theta_p(\widehat{L})$ from each end incident to the puncture p .

Let $\theta := (\theta_p)_{p \in \mathbb{M}_o} : \mathcal{L}_{\mathfrak{sl}_3}^x(\Sigma, \mathbb{Q}) \rightarrow (\mathbb{P}_{\mathbb{Q}}^{\vee})^{\mathbb{M}_o}$.

It is also verified by inspection that

$$\theta_p(\widehat{L}^*) = (\theta_p(\widehat{L}))^* \quad (3.10)$$

holds for all $p \in \mathbb{M}_o$, where the Dynkin involution on the coweights is given by $(\varpi_s^{\vee})^* := \varpi_{3-s}^{\vee}$ for $s = 1, 2$.

3.2.2. *The peripheral action on $\mathcal{L}_{\mathfrak{sl}_3}^a(\Sigma, \mathbb{Q})$.* We have a natural action of $(\mathbb{Q}^2)^{\mathbb{M}}$ on $\mathcal{L}_{\mathfrak{sl}_3}^a(\Sigma, \mathbb{Q})$ that adds peripheral leaves to a given bounded \mathfrak{sl}_3 -lamination. It turns out to be natural to interpret it as actions of the coroot lattice, as follows. For a marked point $m \in \mathbb{M}$, a copy of $\mathbb{Q}_{\mathbb{Q}}^{\vee}$ acts on $\mathcal{L}_{\mathfrak{sl}_3}^a(\Sigma, \mathbb{Q})$, where $\mu = v_1\alpha_1^{\vee} + v_2\alpha_2^{\vee} \in \mathbb{Q}_{\mathbb{Q}}^{\vee}$ adds the peripheral components around m of the following forms:

- oriented counter-clockwisely with weight $2v_1 - v_2$, and
- oriented clockwise with weight $-v_1 + 2v_2$.

This action is designed so that the fundamental coweight $\varpi_1^{\vee} = \frac{1}{3}(2\alpha_1^{\vee} + \alpha_2^{\vee})$ (resp. $\varpi_2^{\vee} = \frac{1}{3}(\alpha_1^{\vee} + 2\alpha_2^{\vee})$) gives rise to a single peripheral component with weight 1 and the counter-clockwise (resp. clockwise) orientation. These actions assigned to the marked points commute with each other. In Section 4.2, we will see that this action coincides with the tropicalization of the $H_{\mathcal{A}}$ -action on the cluster variety $\mathcal{A}_{\mathfrak{sl}_3, \Sigma}$.

3.2.3. *The lamination exact sequence.* The previously discussed structures are combined as follows.

Proposition 3.5. *We have $\theta^{-1}(0) = p(\mathcal{L}_{\mathfrak{sl}_3}^a(\Sigma, \mathbb{Q}))$. Therefore we have the exact sequence*

$$0 \rightarrow (\mathbb{Q}_{\mathbb{Q}}^{\vee})^{\mathbb{M}} \rightarrow \mathcal{L}_{\mathfrak{sl}_3}^a(\Sigma, \mathbb{Q}) \xrightarrow{p} \mathcal{L}_{\mathfrak{sl}_3}^x(\Sigma, \mathbb{Q}) \xrightarrow{\theta} (\mathbb{P}_{\mathbb{Q}}^{\vee})^{\mathbb{M}_o} \rightarrow 0.$$

Here the map $(\mathbb{Q}_{\mathbb{Q}}^{\vee})^{\mathbb{M}} \rightarrow \mathcal{L}_{\mathfrak{sl}_3}^a(\Sigma, \mathbb{Q})$ is given by the action on the empty \mathfrak{sl}_3 -lamination.

Indeed, since a pair of ends with opposite coweights are not allowed by the admissible condition, $\theta^{-1}(0)$ consists of the bounded rational \mathfrak{sl}_3 -laminations, namely the image of p . The exactness of the other parts are obvious.

Let us denote the space of bounded \mathfrak{sl}_3 -laminations without peripheral components by $\mathcal{L}_{\mathfrak{sl}_3}^u(\Sigma, \mathbb{Q}) := \theta^{-1}(0) = p(\mathcal{L}_{\mathfrak{sl}_3}^a(\Sigma, \mathbb{Q}))$. Then we have an obvious splitting

$$(p, (\mathbf{w}_m)_{m \in \mathbb{M}}) : \mathcal{L}_{\mathfrak{sl}_3}^a(\Sigma, \mathbb{Q}) \xrightarrow{\sim} \mathcal{L}_{\mathfrak{sl}_3}^u(\Sigma, \mathbb{Q}) \times (\mathbb{Q}_{\mathbb{Q}}^{\vee})^{\mathbb{M}}, \quad (3.11)$$

where $\mathbf{w}_m : \mathcal{L}_{\mathfrak{sl}_3}^a(\Sigma, \mathbb{Q}) \rightarrow \mathbb{Q}_{\mathbb{Q}}^{\vee}$ extracts the weights of peripheral components around $m \in \mathbb{M}$. We will see that \mathbf{w}_m is given by the tropicalized Goncharov–Shen potential in Proposition 5.12 (cf. [DS20II, Section 2]).

3.3. The spiralling diagram associated with a signed web. In order to define the shear coordinates of a non-elliptic signed web W , we first deform it to the *spiralling diagram* \mathcal{W} . See [IK22, Section 3] for a detail. Roughly speaking, the spiralling diagram \mathcal{W} is obtained as follows.

- (1) In a small disk neighborhood D_p of each puncture $p \in \mathbb{M}_{\circ}$, deform each end of W incident to p into an infinitely spiralling curve, according to their signs as shown in Figure 3.
- (2) The resulting (possibly infinite) self-intersections are replaced with H-shaped parts as shown in Figure 4.

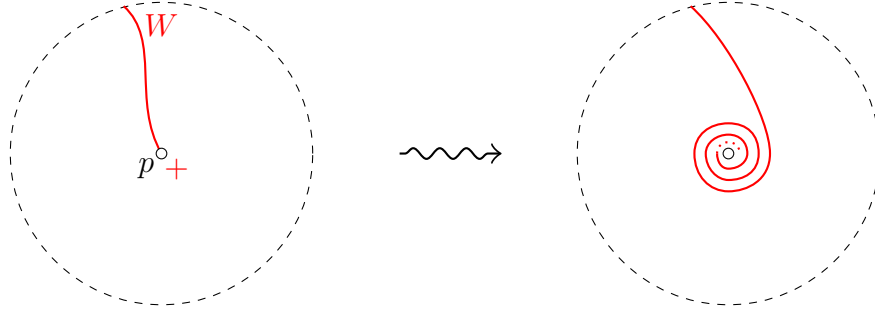


FIGURE 3. Construction of a spiralling diagram. The negative sign similarly produces an end spiralling counter-clockwisely.

Given an ideal triangulation Δ of Σ without self-folded triangles, the associated *split ideal triangulation* $\hat{\Delta}$ is obtained from Δ by replacing each edge E with a biangle B_E . The following is an unbounded version of the notion of *good position* of bounded webs [FS20, DS20I].

Definition 3.6. The spiralling diagram \mathcal{W} is in a *good position* with respect to a split triangulation $\hat{\Delta}$ if the intersection $\mathcal{W} \cap B_E$ (resp. $\mathcal{W} \cap T$) is an unbounded essential (resp. reduced essential) local web ([IK22, Section 3.1]) for each $E \in e(\Delta)$ and $T \in t(\Delta)$.

Here,

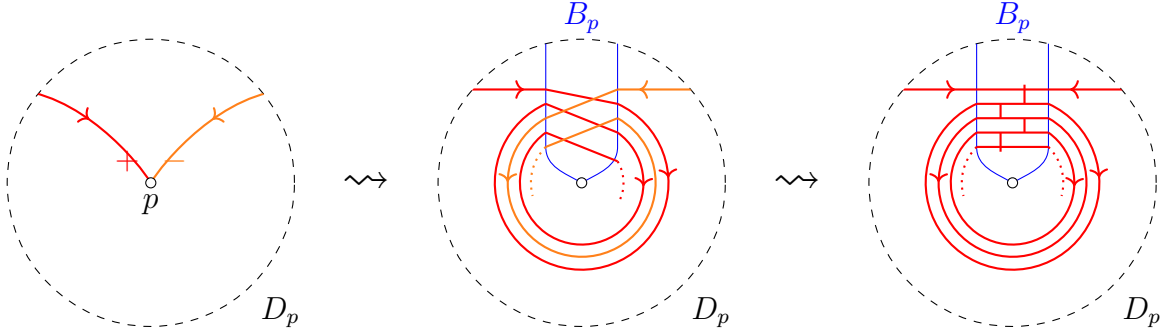


FIGURE 4. Construction of a spiralling diagram. Replace intersections with H-webs in a periodic manner.

- An unbounded essential web on a biangle B is the ladder-web $W(S)$ associated with an asymptotically periodic symmetric strand set S as shown in the left of Figure 5.
- An unbounded reduced essential web on a triangle T is the disjoint union of at most one honeycomb and at most one semi-infinite asymptotically periodic collection of corner arcs around each corner. See right of Figure 5.

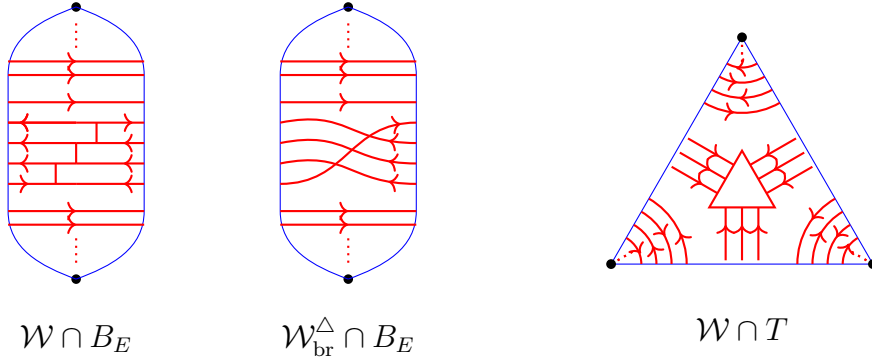


FIGURE 5. Unbounded essential webs on a biangle (Left) and a triangle (Right). The braid representative of the former is shown in the Middle.

Again, see [IK22, Section 3.3] for a detail. Then, after some technical discussion, we can verify that any spiralling diagram arising from a non-elliptic signed web on Σ can be isotoped into a good position with respect to $\hat{\Delta}$ by a finite sequence of certain elementary moves [IK22, Theorem 3.10]. Moreover, such a good position is unique up to certain elementary moves.

While the spiralling diagram itself is suited to discuss its good position, the following *braid representation* will be useful to define the shear coordinates:

Definition 3.7 (Braid representation of a spiralling diagram). Let \mathcal{W} be a spiralling diagram in a good position with respect to $\hat{\Delta}$. Then its *braid representation* $\mathcal{W}_{\text{br}}^{\Delta}$ is

obtained from \mathcal{W} by replacing the unbounded essential web $\mathcal{W} \cap B_E$ on each biangle B_E with its braid representation.

3.4. Shear coordinates. Let us recall the shear coordinates associated with an ideal triangulation Δ of Σ without self-folded triangles. Let $\hat{\Delta}$ be the associated split triangulation.

Given a rational \mathfrak{sl}_3 -lamination $\hat{L} \in \mathcal{L}_{\mathfrak{sl}_3}^x(\Sigma, \mathbb{Q})$, represent it by an \mathfrak{sl}_3 -web W together with rational weights on its components and signs at the ends incident to punctures. Let \mathcal{W} be the associated spiralling diagram together with rational weights on the components, placed in good position with respect to $\hat{\Delta}$. Let $\mathcal{W}_{\text{br}}^\Delta$ be its braid representation, together with well-assigned rational weights on its components. The shear coordinates of \hat{L} are going to be defined out of $\mathcal{W}_{\text{br}}^\Delta$.

For each $E \in e_{\text{int}}(\Delta)$, let Q_E be the unique quadrilateral containing E as its diagonal, regarded as the union of two triangles T_L, T_R and the biangle B_E . By [FS20, Theorem 19] ([DS20I, Proposition 22]), the restriction of $\mathcal{W}_{\text{br}}^\Delta$ to each of T_L and T_R has at most one honeycomb web, which is represented by a triangular symbol as in Notation 3.2. We call any strand in the braid representative $\mathcal{W}_{\text{br}}^\Delta \cap Q_E$ that is incident to the triangular symbol in T_L (if exists) a T_L -strand. Similarly, we define T_R -strands. It is possible that an arc is both T_L - and T_R -strand, in which case it connects the two honeycombs. By removing the T_L - and T_R -strands, the remaining is a collection of (possibly intersecting) oriented curves, which we call the *curve components*.

Definition 3.8 (\mathfrak{sl}_3 -shear coordinates). The (\mathfrak{sl}_3) -shear coordinate system

$$\mathbf{x}_\Delta^{\text{uf}}(\hat{L}) = (\mathbf{x}_i^\Delta(\hat{L}))_{i \in I_{\text{uf}}(\Delta)} \in \mathbb{Q}^{I_{\text{uf}}(\Delta)}$$

is defined as follows. First, for each $E \in e_{\text{int}}(\Delta)$, the coordinates assigned to the four vertices in the interior of Q_E only depend on the restriction $\mathcal{W}_{\text{br}}^\Delta \cap Q_E$.

- (1) Each curve component contributes to the edge coordinates according to the rule shown in Figure 6.
- (2) The honeycomb on the triangle T_L contributes to $\mathbf{x}_\Delta^{\text{uf}}(\hat{L})$ as in Figure 7. Namely, the face coordinate counts the height of the honeycomb web, where a sink (resp. source) is counted positively (resp. negatively). The edge coordinates count the contributions from T_L -strands, where we have n_1 left-turning ones, n_2 straight-going ones (which are also T_R -strands), and n_3 right-turning ones.
- (3) The honeycomb on the triangle T_R and the T_R -strands contribute in the symmetric way with respect to the π rotation of the figure.

Then the shear coordinates are defined to be the weighted sums of these contributions.

Remark 3.9. The shear coordinates of the first honeycomb component shown in Figure 7 is the same as the sum of shear coordinates of the three honeycomb components shown in Figure 8.

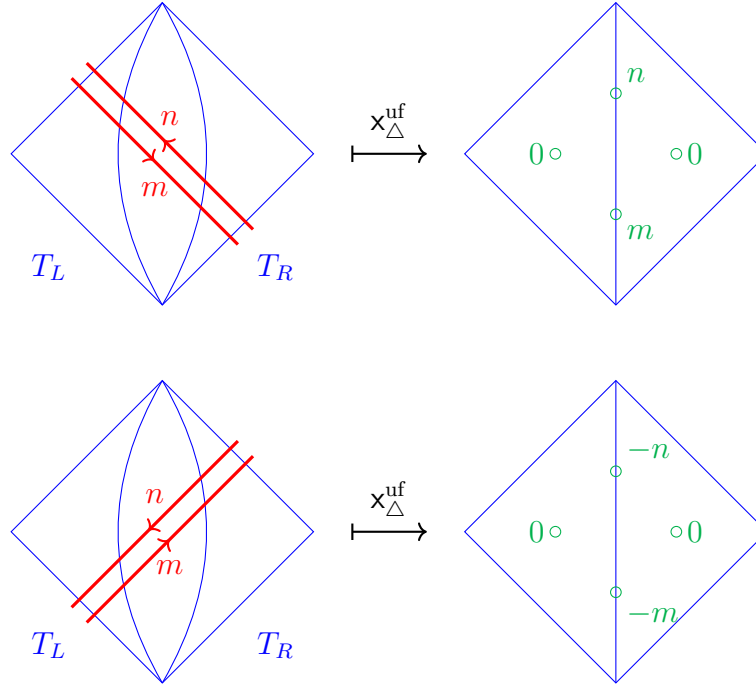
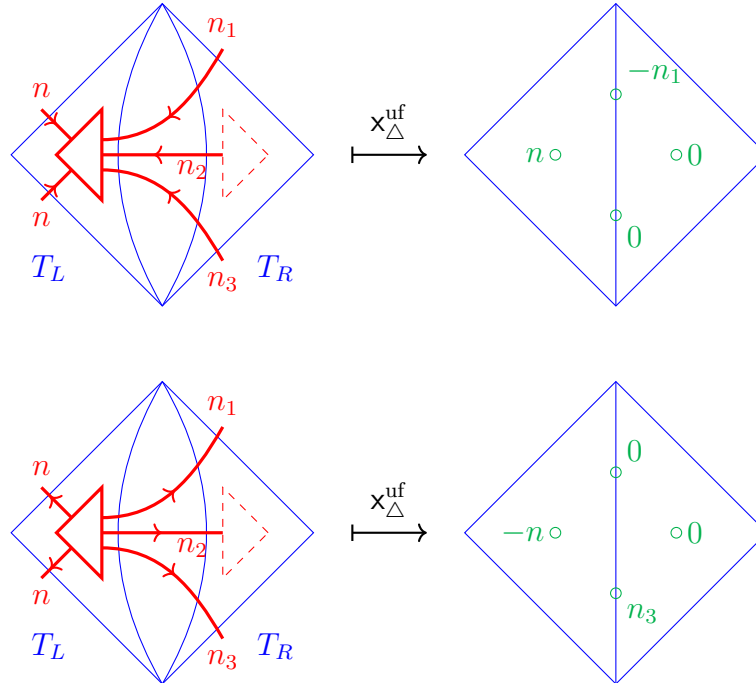


FIGURE 6. Contributions from curve components.

FIGURE 7. Contributions from the honeycomb of height $n = n_1 + n_2 + n_3$ on the triangle T_L . Observe that the n_2 straight-going T_L -strands do not contribute.

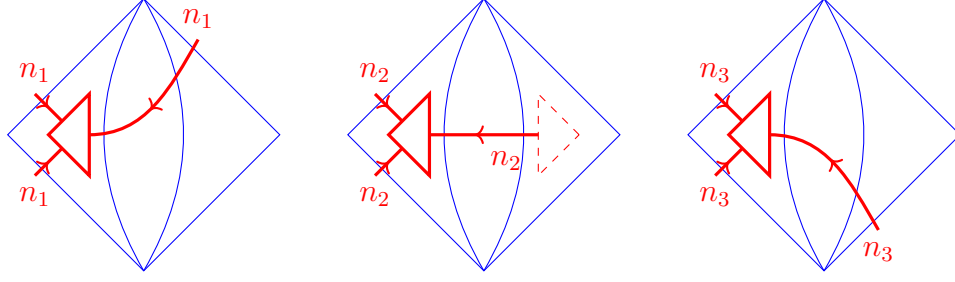


FIGURE 8. Basic honeycomb components

Theorem 3.10 ([IK22, Theorem 1]). *The shear coordinate system $\mathbf{x}_\Delta^{\text{uf}}(\widehat{L}) \in \mathbb{Q}^{I_{\text{uf}}(\Delta)}$ gives a well-defined bijection*

$$\mathbf{x}_\Delta^{\text{uf}} : \mathcal{L}_{\mathfrak{sl}_3}^x(\Sigma, \mathbb{Q}) \rightarrow \mathbb{Q}^{I_{\text{uf}}(\Delta)}.$$

Moreover, for any another ideal triangulation Δ' of Σ , the coordinate transformation $\mathbf{x}_{\Delta'} \circ \mathbf{x}_\Delta^{-1}$ is a composite of tropical cluster \mathcal{X} -transformations.

As a consequence, the shear coordinates combine to give an $MC(\Sigma)$ -equivariant bijection

$$\mathbf{x}_\bullet^{\text{uf}} : \mathcal{L}_{\mathfrak{sl}_3}^x(\Sigma, \mathbb{Q}) \xrightarrow{\sim} \mathcal{X}_{\mathfrak{sl}_3, \Sigma}^{\text{uf}}(\mathbb{Q}^T). \quad (3.12)$$

In other words, the space $\mathcal{L}_{\mathfrak{sl}_3}^x(\Sigma, \mathbb{Q})$ can be viewed as a tropical analogue of the moduli space $\mathcal{X}_{PGL_3, \Sigma}$ of framed PGL_3 -local systems [FG06a] with respect to its positive structure.

Notation 3.11. We will write $\mathbf{x}_T^\Delta := \mathbf{x}_{i(T)}^\Delta$ for a triangle T of Δ , and $\mathbf{x}_{E,s}^\Delta := \mathbf{x}_{i^s(E)}^\Delta$ for an oriented edge E of Δ and $s = 1, 2$. Here recall the notations in Section 2.1.

Dynkin involution. At the rest of this section, we recall the equivariance of the shear coordinates under the Dynkin involution (Definition 3.3). The *cluster action* $*_\Delta$ (see the last paragraph of Appendix A) of the Dynkin involution in the cluster chart associated to Δ is given by some mutation sequence, and it induces the tropical cluster \mathcal{X} -transformation

$$\begin{aligned} *_\Delta^x : \mathbf{x}_T &\mapsto -\mathbf{x}_T, & \text{for } T \in t(\Delta), \\ \mathbf{x}_{E,1} &\mapsto \mathbf{x}_{E,2} + [\mathbf{x}_{T_L}]_+ - [-\mathbf{x}_{T_R}]_+, \\ \mathbf{x}_{E,2} &\mapsto \mathbf{x}_{E,1} + [\mathbf{x}_{T_R}]_+ - [-\mathbf{x}_{T_L}]_+ & \text{for } E \in e(\Delta). \end{aligned}$$

Proposition 3.12 ([IK22, Proposition 4.13]). *We have the commutative diagram*

$$\begin{array}{ccc} \mathcal{L}_{\mathfrak{sl}_3}^x(\Sigma, \mathbb{Q}) & \xrightarrow{\mathbf{x}_\Delta} & \mathbb{Q}^{I_{\text{uf}}(\Delta)} \\ * \downarrow & & \downarrow *_\Delta \\ \mathcal{L}_{\mathfrak{sl}_3}^x(\Sigma, \mathbb{Q}) & \xrightarrow{\mathbf{x}_\Delta} & \mathbb{Q}^{I_{\text{uf}}(\Delta)}. \end{array}$$

In particular, the orientation-reversing action of the Dynkin involution coincides with the cluster action.

4. STRUCTURE OF UNBOUNDED \mathfrak{sl}_3 -LAMINATIONS AROUND PUNCTURES

4.1. Classification of unbounded \mathfrak{sl}_3 -laminations around punctures. In this section, we focus on the rational unbounded \mathfrak{sl}_3 -laminations around a puncture as a preparation for the study of the cluster exact sequence and the Weyl group actions at punctures in the subsequent sections.

Let us first clarify the elementary pieces that we are going to classify. Fix an ideal triangulation Δ of a marked surface Σ . Given a non-elliptic signed web W on Σ , let \mathcal{W} be the associated spiralling diagram in a good position with respect to $\widehat{\Delta}$, and $\mathcal{W}_{\text{br}}^\Delta$ its braid representation. Recall that each of the shear coordinates of W is defined to be a sum of contributions from the components of $\mathcal{W}_{\text{br}}^\Delta$ (Figures 6 and 7).

In view of the rules in Figure 7, we can further decompose the contributions from honeycomb components as follows. For each triangle $T \in t(\Delta)$, split a honeycomb of height n into a union of n honeycombs of height one. See Figure 9 for an example. Then $\mathcal{W}_{\text{br}}^\Delta$ is decomposed into a union $\mathcal{W}_{\text{br}}^\Delta = \bigcup_\alpha \mathcal{W}_\alpha$ of webs only with honeycombs of height one. Let us call each web \mathcal{W}_α appearing in this decomposition an *elementary braid* with respect to Δ . Let W_α denote the signed web corresponding to \mathcal{W}_α .

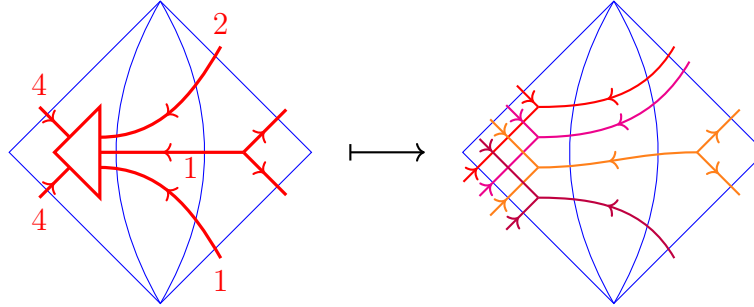


FIGURE 9. Decomposition of a braid component into elementary braids.

Lemma 4.1. *The shear coordinates of W can be computed as sums of contributions from elementary braids:*

$$x_i^\Delta(W) = \sum_{\alpha} x_i^\Delta(W_\alpha)$$

for $i \in I_{\text{uf}}(\Delta)$. Moreover, the signs of shear coordinates are coherent: $x_i^\Delta(W_\alpha) \cdot x_i^\Delta(W_{\alpha'}) \geq 0$ for $i \in I(\Delta)$ and $\alpha \neq \alpha'$.

Proof. The first assertion follows from Remark 3.9. The signs of face coordinates $x_T^\Delta(W_\alpha)$, $T \in t(\Delta)$ are coherent since the original web W has a sink (resp. source) honeycomb if and only if each W_α has a sink (resp. source) honeycomb.

For the edge coordinates, let us focus on the quadrilateral shown in Figures 6 and 7. If there were two elementary braids which contribute positively and negatively to the same edge coordinate, then they would have an intersection inside the bigon B_E with

the same orientation (in the sense ‘left-to-right’ or ‘right-to-left’). It contradicts to the construction of the braid representative (see also the left picture in Figure 5). Hence we have $\mathbf{x}_i^\Delta(W_\alpha) \cdot \mathbf{x}_i^\Delta(W_{\alpha'}) \geq 0$ for all $i \in I_{\text{uf}}(\Delta)$. \blacksquare

Let D^* be a once-punctured disk with two special points, together with the ideal triangulation shown in Figure 10.

Proposition 4.2 (Classification of elementary braids on D^*). *All possible elementary braids on D^* are the eleven ones shown in Figure 10, up to orientation-reversion and the π -rotation.*

Proof. By cutting D^* along one of the interior edges, say E , we get a quadrilateral. Then by the discussion in the beginning of Section 3.4, $\mathcal{W}_{\text{br}} \setminus E$ has at most two honeycomb components, and the other parts are curve components. For elementary braids, these honeycomb components have height 1. Then we consider all possible patterns to connect them across the edge E . Those arising from the curve components are listed in the top row of Figure 10. The second and third rows exhaust all the patterns with one and two honeycomb components, respectively. \blacksquare

Remark 4.3. Thanks to the sign coherence statement in Lemma 4.1, we can reduce the computations of a piecewise linear map (such as a cluster transformation) to that for the elementary braids, whenever its bending loci are of the form $\mathbf{x}_i^\Delta = 0$. It will be useful, for example in the proof of Theorem 5.11.

4.2. Equivalence to the cluster exact sequence. Here we compare the lamination exact sequence in Proposition 3.5 with the tropicalization of the cluster exact sequence [FG09] (see Appendix A). Recall that for each puncture $p \in \mathbb{M}_o$, associated is the tropicalized Casimir functions $\theta_p : \mathcal{L}_{\mathfrak{sl}_3}^x(\Sigma, \mathbb{Q}) \rightarrow \mathbb{P}_{\mathbb{Q}}^\vee$. Let $\langle \cdot, \cdot \rangle : \mathbb{Q}_{\mathbb{Q}} \otimes \mathbb{P}_{\mathbb{Q}}^\vee \rightarrow \mathbb{Q}$ denote the dual pairing, for which we have $\langle \alpha_s, \varpi_t^\vee \rangle = \delta_{st}$. Take an ideal triangulation $\Delta(p)$ of Σ so that the star neighborhood of p is a once-punctured disk with two marked points on its boundary. Label the vertices of the quiver $Q^{\Delta(p)}$ as prescribed in Figure 11.

Proposition 4.4. *We have*

$$\begin{aligned} \langle \alpha_1, \mathbf{x}_{\Delta(p)}^* \theta_p \rangle &= \mathbf{x}_3 + \mathbf{x}_4 + \mathbf{x}_5 + \mathbf{x}_6, \\ \langle \alpha_2, \mathbf{x}_{\Delta(p)}^* \theta_p \rangle &= \mathbf{x}_1 + \mathbf{x}_2. \end{aligned}$$

In particular, the map θ_p is identified with the tropicalization of the cluster Casimir map $\theta : \mathcal{X}_{\mathfrak{sl}_3, \Sigma} \rightarrow H_{\mathcal{X}}$ (Appendix A.2).

Proof. By the $\mathbb{Q}_{>0}$ -equivariance, it suffices to show the equations for integral \mathfrak{sl}_3 -lamination. Let \widehat{L} be an integral \mathfrak{sl}_3 -lamination represented by a non-elliptic signed web W , and \mathcal{W} the associated spiralling diagram in good position with respect to the split triangulation $\widehat{\Delta}(p)$. Since both sides of the equations only depend on the restriction of \mathcal{W} to the

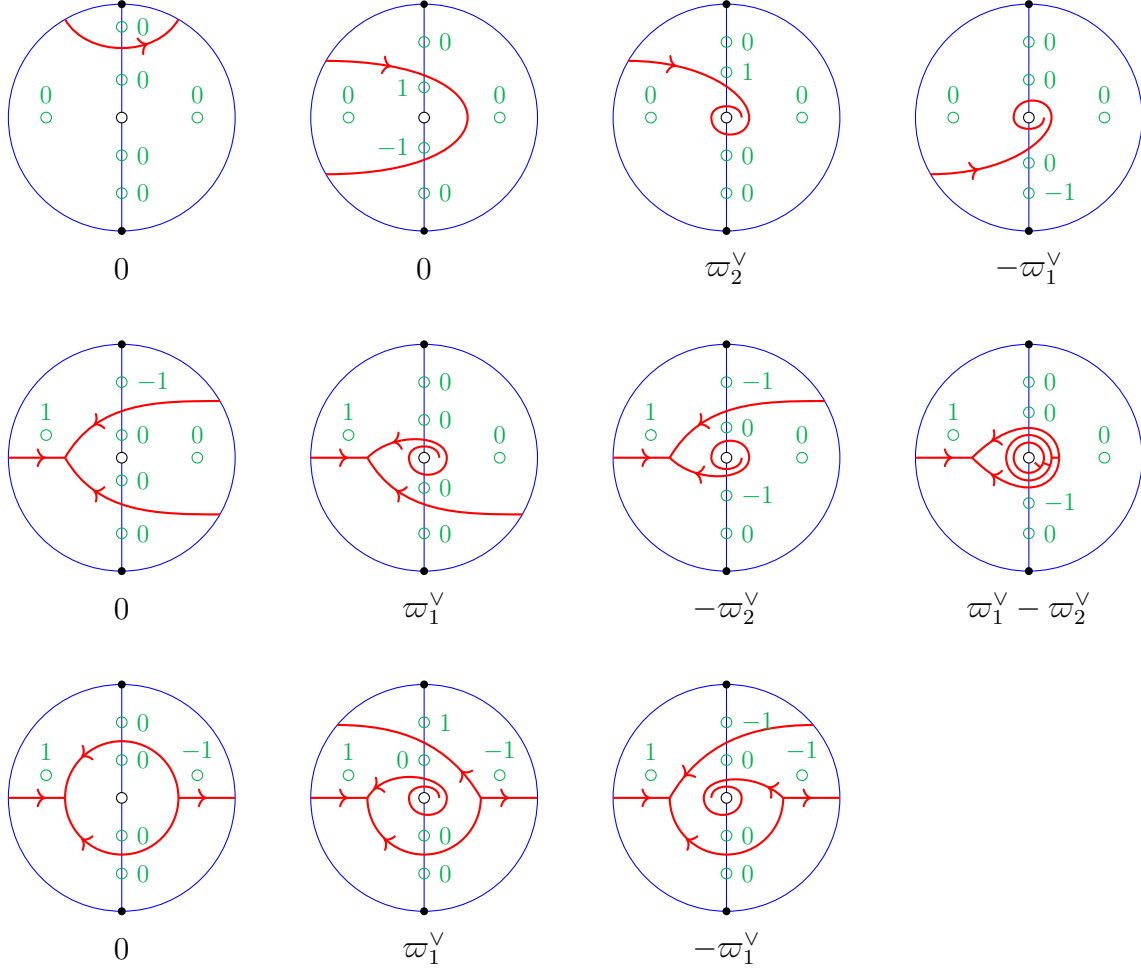


FIGURE 10. Elementary braids on D^* and their shear coordinates. Below each picture, shown is the value of the tropicalized Casimir function assigned at the central puncture.

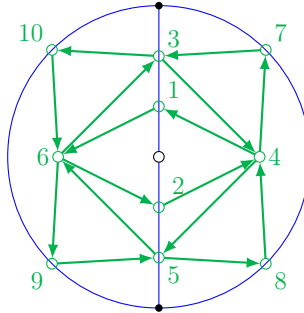


FIGURE 11. The quiver $Q^{\Delta(p)}$ around a puncture p . Here possible (half-) arrows between boundary vertices are omitted.

once-punctured disk $D^*(p)$ containing the puncture p with two special points, we can concentrate on the diagram $\mathcal{W}_p := \mathcal{W} \cap D^*(p)$. Then it suffices to consider the elementary

braids listed in Figure 10, for which one can easily verify the desired equations. The cases for the opposite orientation can be similarly verified, or one can deduce them by applying (3.10) and Proposition 3.12. The assertion is proved. \blacksquare

Theorem 4.5. *The sequence*

$$0 \rightarrow H_{\mathcal{A}}(\mathbb{Q}^T) \rightarrow \mathcal{L}_{\mathfrak{sl}_3}^a(\Sigma, \mathbb{Q}) \xrightarrow{p} \mathcal{L}_{\mathfrak{sl}_3}^x(\Sigma, \mathbb{Q}) \xrightarrow{\theta} H_{\mathcal{X}}(\mathbb{Q}^T) \rightarrow 0$$

of PL maps (Proposition 3.5) coincides with the cluster exact sequence (A.9).

Proof. By Lemmas A.1 and A.2, the \mathbb{Q} -vector spaces $H_{\mathcal{X}}(\mathbb{Q}^T)$ and $H_{\mathcal{A}}(\mathbb{Q}^T)$ introduced in Section 3.2 are the same as the tropicalizations of the tori $H_{\mathcal{X}}$ and $H_{\mathcal{A}}$, respectively. Moreover, the ensemble map $p : \mathcal{L}_{\mathfrak{sl}_3}^a(\Sigma, \mathbb{Q}) \rightarrow \mathcal{L}_{\mathfrak{sl}_3}^x(\Sigma, \mathbb{Q})$ and the tropicalized Casimir map $\theta : \mathcal{L}_{\mathfrak{sl}_3}^x(\Sigma, \mathbb{Q}) \rightarrow H_{\mathcal{X}}(\mathbb{Q}^T)$ coincide with the cluster ones by [IK22, Proposition 4.10] and Proposition 4.4, respectively. It remains to show that the $\mathbb{Q}_{\mathbb{Q}}^{\vee}$ -action adding peripheral components around a marked point $m \in \mathbb{M}$ coincides with the tropicalization of the cluster action of $H_{\mathcal{A}}$ on $\mathcal{A}_{\mathfrak{sl}_3, \Sigma}$.

For a puncture $p \in \mathbb{M}_o$, take a labeled \mathfrak{sl}_3 -triangulation $(\Delta(p), \ell(p))$ as in Figure 11. Then the peripheral components around p with weight 1 have the shear coordinates as shown in Figure 12. In particular, given any \mathfrak{sl}_3 -lamination $\tilde{L} \in \mathcal{L}_{\mathfrak{sl}_3}^a(\Sigma, \mathbb{Q})$, the action adding the peripheral component around p with weight $t \in \mathbb{Q}$ and counter-clockwise orientation shifts the tropical \mathcal{A} -coordinates as

$$\mathbf{a}_i(\tilde{L}) \mapsto \begin{cases} \mathbf{a}_i(\tilde{L}) + \frac{2}{3}t, & \text{if } i = 3, 4, 5, 6, \\ \mathbf{a}_i(\tilde{L}) + \frac{1}{3}t, & \text{if } i = 1, 2, \\ \mathbf{a}_i(\tilde{L}) & \text{otherwise.} \end{cases}$$

This is exactly the tropicalized version of the cluster action (A.3) induced by the element $\varpi_1^{\vee} = \frac{2}{3}\alpha_1^{\vee} + \frac{1}{3}\alpha_2^{\vee} \in K_{\mathbb{Q}}^{\vee}$. Similarly, the action adding the peripheral component with clockwise orientation coincides with the tropicalized action given by $\varpi_2^{\vee} = \frac{1}{3}\alpha_1^{\vee} + \frac{2}{3}\alpha_2^{\vee} \in K^{\vee}$. Thus the $\mathbb{Q}_{\mathbb{Q}}^{\vee}$ -action in Proposition 3.5 associated with the puncture p coincides with the cluster action. The coincidence of two actions associated with a special point is similarly verified. \blacksquare

Remark 4.6. The action given by $\beta \in H_{\mathcal{A}}(\mathbb{Q}^T)$ preserves the integral part $\mathcal{L}_{\mathfrak{sl}_3}^a(\Sigma, \mathbb{Z})$ if and only if it belongs to the coroot lattices.

5. WEYL GROUP ACTIONS AT PUNCTURES

We are going to introduce an action of the Weyl group of the Lie algebra \mathfrak{sl}_3 at each puncture $p \in \mathbb{M}_o$ and investigate its cluster nature. The action is defined so that the tropicalized Casimir function $\theta_p : \mathcal{L}_{\mathfrak{sl}_3}^x(\Sigma, \mathbb{Q}) \rightarrow H_{\mathcal{X}}(\mathbb{Q}^T)$ is equivariant under this action. While this is a natural requirement which uniquely determines the action on each signed end of a given unbounded \mathfrak{sl}_3 -lamination, it turns out that it in general leads to resolvable

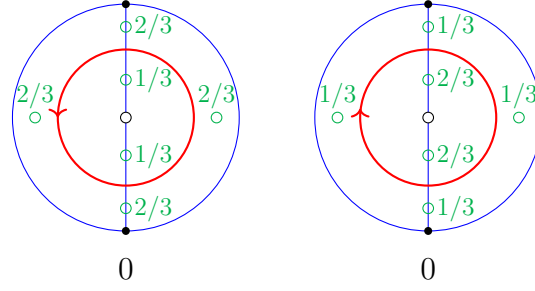


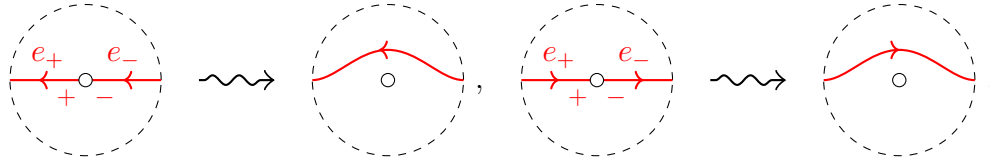
FIGURE 12. The shear coordinates of peripheral components around a puncture p .

pairs in (3.3) that we have excluded: the reader is recommended to quickly see Definition 5.7 and Proposition 5.9. Therefore we begin with brief discussion on signed webs with resolvable pairs (but still without the latter two types of bad ends in (3.3)) and a new operation that allows us to reduce such a web to an ordinary signed web. Observe that the spiralling diagram \mathcal{W} can be defined without any modification, and hence we can also define the shear coordinates for such a signed web.

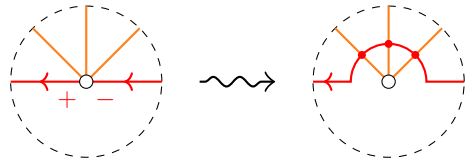
5.1. Resolution of resolvable pairs.

Definition 5.1 (resolution of resolvable pairs). Let W be a non-elliptic signed web with resolvable pairs at a puncture $p \in \mathbb{M}_0$.

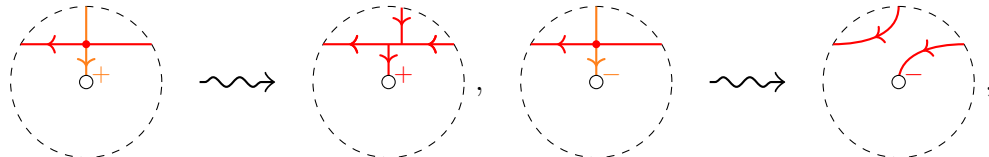
Step 0: Assume first that W has exactly one resolvable pair (e_+, e_-) at p , and there is no other ends incident to p . The basic idea is that we resolve the pair $(e_+ e_-)$ in the following way:

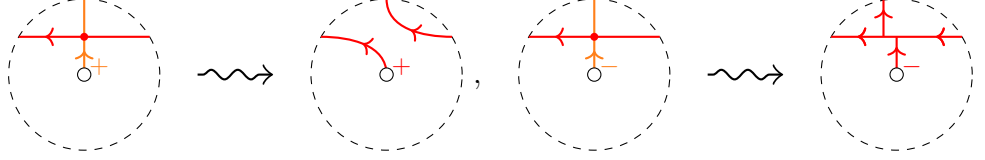


Step 1: In general, let (e_+, e_-) be a resolvable pair at p among the other ends incident to p . Then the above resolution rule will produce intersections with the other signed ends, and give rise to a signed web with self-intersections:



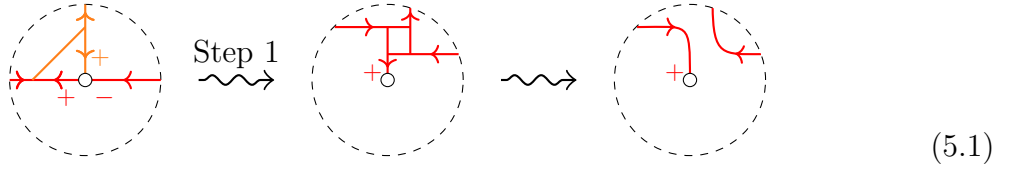
Here the chosen resolvable pair is shown in red. Then we resolve each intersection in the following way (in the order from the farthest from p):



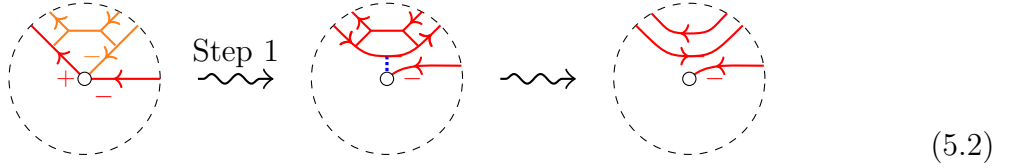


The rule is extended by equivariance under the Dynkin involution.

Step 2: The resulting signed web may have 2-gon or 4-gon faces. We eliminate the 2-gon faces naturally as in the skein relation [IK22, (5.4)]. The 4-gon face can only arise from a 3-gon face or a 5-gon face in the original signed web. We remove such a 4-gon face in the following way:



(5.1)



(5.2)

Here it is crucial to remember the puncture from which the 4-gon arose (indicated by a dotted blue line in (5.2)) to determine the direction of removal.

We call the above process the *resolution of the resolvable pair* (e_+, e_-) at p , and the resulting signed web is denoted by $W_{(e_+, e_-)}$.

Note that $W_{(e_+, e_-)}$ has a less number of resolvable pairs than the original signed web W .

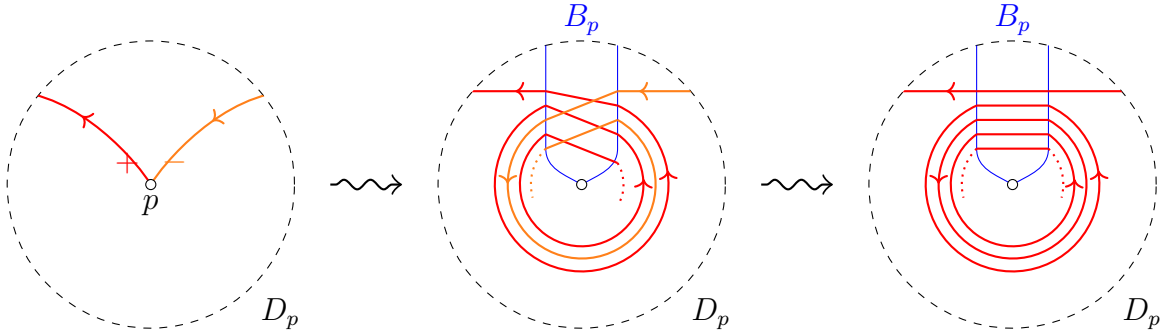
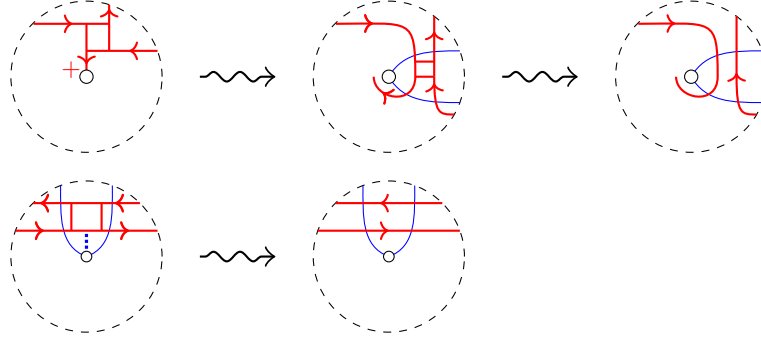


FIGURE 13. Spiralling diagram associated with a resolvable pair. Observe that the middle one is not the ladder-web associated with the asymptotically periodic symmetric strand set on B_p , and thus replaced with the right one.

Remark 5.2. The basic ideas of the rules in Definition 5.1 are as follows. Firstly, one can naively consider a spiralling diagram to a signed web with resolvable pairs just as before.

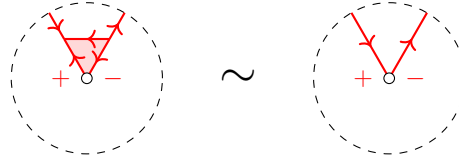
The operation in Step 0 is designed so that it preserves such spiralling diagrams: see Figure 13. Step 1 also preserves the spiralling diagrams, which can be verified similarly as in the proof of the well-definedness of the shear coordinates [IK22, Proposition 3.14] by choosing an appropriate biangle.

Although the resolution direction of a 4-gon face is not determined by the skein point of view, the spiralling direction tells us the correct way. Indeed, one can push any 4-gon arising from Step 1 into the chosen biangle, as follows:

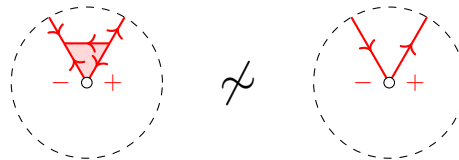


This is exactly the rules in Step 2.

Remark 5.3. From the 2-gon elimination rule in Step 2, we get the following additional puncture H-move:



and similarly for the opposite orientation. Here \sim means that both the signed webs produce the same non-elliptic admissible signed web after the resolution procedure. It preserves the associated spiralling diagrams. On the other hand, a similar move with the opposite signs shown below is not allowed, since it neither preserves the associated spiralling diagrams nor compatible with the resolution procedure.



The following proposition states that the resolution procedure does not affect the shear coordinates and that after a successive application of these procedures, we eventually get a unique non-elliptic signed web without resolvable pairs.

Proposition 5.4 (Proof in Section 5.3). *(1) The resolution operations are associative. Namely, we have*

$$(W_{(e_+, e_-)})(e'_+, e'_-) = (W_{(e'_+, e'_-)})(e_+, e_-)$$

up to isotopy for any resolvable pairs (e_+, e_-) , (e'_+, e'_-) at distinct punctures $p \neq p' \in \mathbb{M}_o$, respectively. When $p = p'$, we have

$$\begin{aligned} (W_{(e_+, e_-)})(e'_+, e'_-) &= (W_{(e'_+, e'_-)})(e_+, e_-) && \text{if } e_+ \neq e'_+ \text{ and } e_- \neq e'_-, \\ W_{(e_+, e_-)} &= W_{(e'_+, e_-)} && \text{if } e'_- = e_-, \\ W_{(e_+, e_-)} &= W_{(e_+, e'_-)} && \text{if } e'_+ = e_+ \end{aligned}$$

up to isotopy. As a consequence of these properties, we get a unique non-elliptic admissible signed web W^{red} obtained from W by successively applying the resolution operations in any order.

- (2) If two non-elliptic signed webs W_1, W_2 are transformed to each other by a sequence of the elementary moves (E1)–(E4), then the non-elliptic admissible signed webs W_1^{red} and W_2^{red} are transformed to each other by a sequence of these moves.

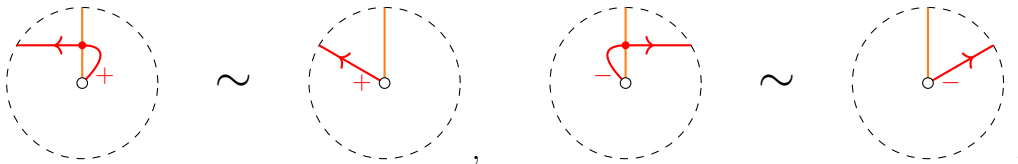
A proof is given in Section 5.3. Let us call a signed web drawn in a small neighborhood of p possibly with finitely many self-intersections a *generalized signed web* near p . In the resolution process, we at once produce a generalized signed web near p in Step 1, and then remove all of its self-intersections according to the local rule specified in Step 2. Observe that:

- it makes sense to remove only a subset of self-intersections to get another generalized signed web;
- the resolution Step 1 for another resolvable pair can be further applied to a generalized signed web before removing all of its self-intersections.

We say that two generalized signed webs are equivalent if they produce equivalent signed webs after resolving all their self-intersections, where we remove the self-intersections from the farthest one from p . It turns out that it is easier to verify the statement (2) in Proposition 5.4 in the level of generalized signed webs. The following lemma is also stated in the level of generalized signed webs.

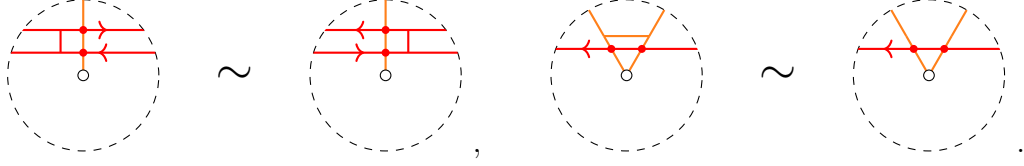
Lemma 5.5 (Proof in Section 5.3). *We have the following equivalences of generalized signed webs:*

(1)



Here the ends shown in orange have any possible orientations and signs.

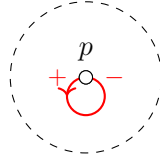
(2)



Here again, the ends shown in orange have any possible orientations and signs. Similarly for their orientation-reversions.

The following lemma is also useful:

Lemma 5.6 (Proof in Section 5.3). *A component C of the form*



can be removed from a signed web W without changing the other components.

These lemmas are also proved in Section 5.3.

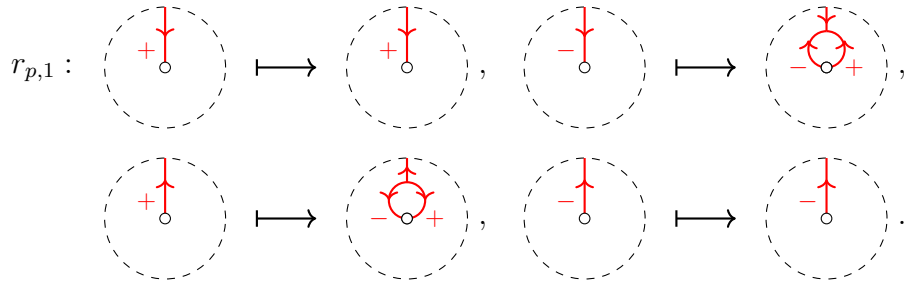
5.2. Weyl group action. Recall that the *Weyl group* $W(\mathfrak{sl}_3)$ is the group presented as

$$W(\mathfrak{sl}_3) = \langle r_1, r_2 \mid r_1^2 = r_2^2 = 1, r_1 r_2 r_1 = r_2 r_1 r_2 \rangle.$$

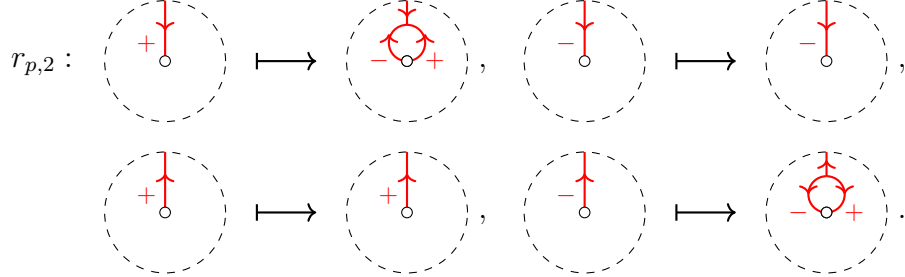
Its natural action on the coweight lattice \mathbf{P}^\vee is given by $r_s \cdot \varpi_t^\vee := \varpi_t^\vee - \delta_{st} \alpha_s^\vee$ for $s, t = 1, 2$. Explicitly,

$$\begin{aligned} r_1 \cdot \varpi_1^\vee &= -\varpi_1^\vee + \varpi_2^\vee, & r_1 \cdot \varpi_2^\vee &= \varpi_2^\vee, \\ r_2 \cdot \varpi_1^\vee &= \varpi_1^\vee, & r_2 \cdot \varpi_2^\vee &= \varpi_1^\vee - \varpi_2^\vee. \end{aligned}$$

Definition 5.7 (reflections at punctures). (1) Let W be a non-elliptic signed web, $p \in \mathbb{M}_\circ$ a puncture. We define two non-elliptic signed webs $r_{p,1}(W)$, $r_{p,2}(W)$ in the following way. First, we keep the part of W outside a small disk neighborhood of p intact. For the first reflection $r_{p,1}$, replace each signed end incident to p by the following rule:



Then we get a generalized signed web W_1 . We define $r_{p,1}(W) := W_1^{\text{red}}$. Similarly for the second reflection $r_{p,2}$, replace each signed end incident to p by the following rule:



Then we get a generalized signed web W_2 , and set $r_{p,2}(W) := W_2^{\text{red}}$.

- (2) Given an integral \mathfrak{sl}_3 -lamination $\widehat{L} \in \mathcal{L}_{\mathfrak{sl}_3}^x(\Sigma, \mathbb{Z})$ represented by a non-elliptic signed web W , define $r_{p,s}(\widehat{L}) := [r_{p,s}(W)]$ for $p \in \mathbb{M}_o$ and $s \in \{1, 2\}$. It is well-defined, thanks to Proposition 5.4 (3). Extend $r_{p,s}$ to be an automorphism on $\mathcal{L}_{\mathfrak{sl}_3}^x(\Sigma, \mathbb{Q})$ by $\mathbb{Q}_{>0}$ -equivariance.

The following is easily verified by inspection:

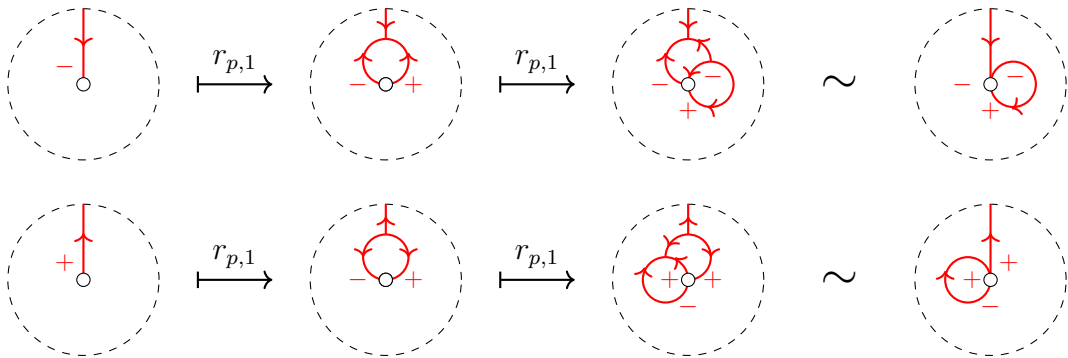
Lemma 5.8. *For each $p \in \mathbb{M}_o$ and $s \in \{1, 2\}$, we have*

$$* \circ r_{p,s} \circ * = r_{p,3-s}$$

as automorphisms on $\mathcal{L}_{\mathfrak{sl}_3}^x(\Sigma, \mathbb{Q})$.

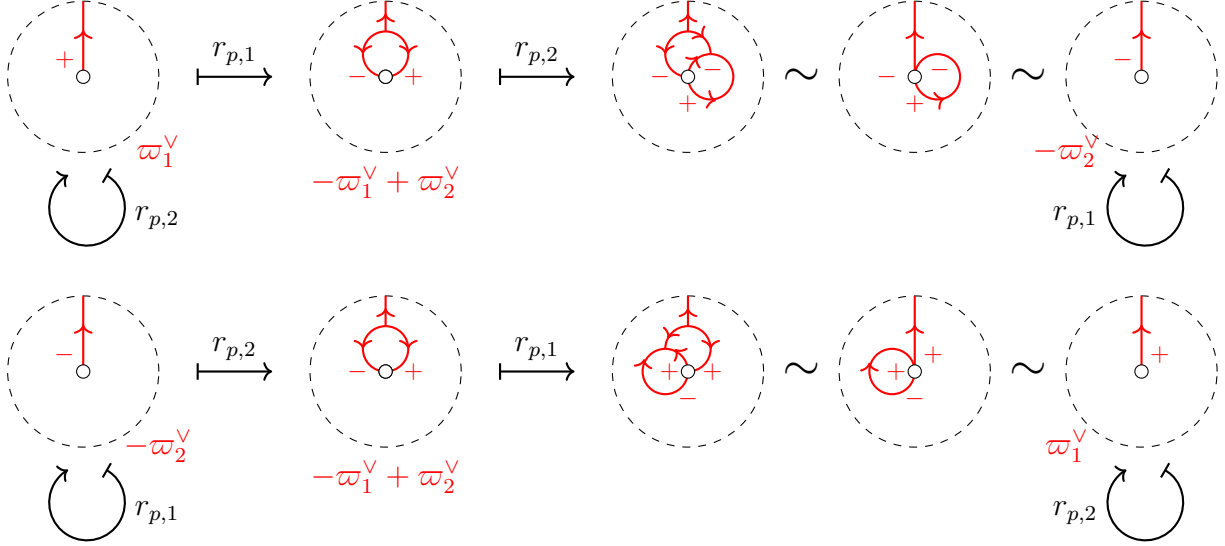
Proposition 5.9. *The above rule defines an action α_p of the Weyl group $W(\mathfrak{sl}_3)$ on $\mathcal{L}_{\mathfrak{sl}_3}^x(\Sigma, \mathbb{Q})$ by setting $\alpha_p(r_s) := r_{p,s}$ for $s = 1, 2$. These actions commute with each other for $p \in \mathbb{M}_o$, and thus induce an action of the direct product $W(\mathfrak{sl}_3)^{\mathbb{M}_o}$.*

Proof. For each $p \in \mathbb{M}_o$, we need to check that the automorphisms $r_{p,1}$ and $r_{p,2}$ satisfy the defining relations of $W(\mathfrak{sl}_3)$. For the involutivity relation $(r_{p,1})^2 = \text{id}$, the non-trivial patterns are the followings:



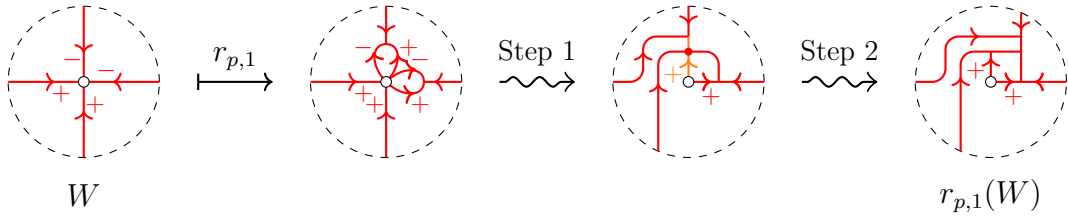
Here we used the puncture H-move (3.6) in the last step. Observe that these operations can be performed inside a small sector containing the original end, and the additional loop based at p can be removed without affecting the possibly existing other ends (not

shown in the figures above) by Lemma 5.6. Thus we get $(r_{p,1})^2 = \text{id}$ from the end-wise verification. Then we also have $(r_{p,2})^2 = \text{id}$ by the $*$ -equivariance (Lemma 5.8). The braid relation $r_{p,1}r_{p,2}r_{p,1} = r_{p,2}r_{p,1}r_{p,2}$ is verified as follows:



Here the values of θ_p are shown for a comparison with the usual action of $W(\mathfrak{sl}_3)$ on the coweight lattice. From these computations we see that the braid relation holds for these two types of ends, and also for the other types by the $*$ -equivariance (Lemma 5.8). Again, thanks to Lemma 5.6, the end-wise verification suffices to prove the assertion. ■

Example 5.10. Here is an example for which we need to apply the resolution move in a non-trivial way:



Recall from (A.7) that the cluster action of the Weyl group $W(\mathfrak{sl}_3)$ assigned at a puncture p is described by the mutation sequence

$$\begin{aligned}\mu_{\gamma_{p,1}} &:= \mu_3\mu_4\mu_5(5\ 6)\mu_5\mu_4\mu_3, \\ \mu_{\gamma_{p,2}} &:= \mu_1(1\ 2)\mu_1,\end{aligned}$$

where we use the local labeling shown in Figure 11. The induced tropical cluster transformations can be computed from [GS18, Theorem 7.7]. For example, $r_{p,2}$ induces

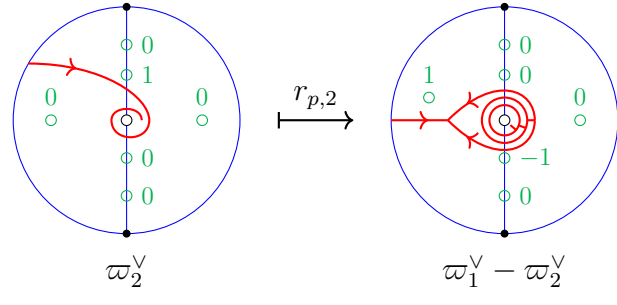
$$\begin{aligned}
 (r_{p,2})_{\Delta(p)} : x_1 &\mapsto -x_2, \\
 x_2 &\mapsto -x_1, \\
 x_4 &\mapsto x_4 - [-x_1]_+ + [x_2]_+, \\
 x_6 &\mapsto x_6 + [x_1]_+ - [-x_2]_+, \\
 x_i &\mapsto x_i \quad \text{for } i \neq 1, 2, 4, 6
 \end{aligned} \tag{5.3}$$

in the cluster chart associated with any triangulation Δ that restricts to $\Delta(p)$.

Theorem 5.11. *The action of $W(\mathfrak{sl}_3)^{\mathbb{M}_o}$ given in Proposition 5.9 coincides with the cluster action.*

Proof. Let us consider the reflection $r_{p,2}$. By Lemma 4.1, it suffices to consider the elementary braids around p shown in Figure 10, and their orientation-reversals. Indeed, the cluster action of $r_{p,2}$ is linear for the coordinate contributions from elementary braids, thanks to the sign coherence statement in Lemma 4.1.

Notice that if $\langle \alpha_2, \theta_p \rangle = 0$, then the reflection $r_{p,2}$ acts on that pattern trivially. On the other hand, one can easily see $x_1 = x_2 = 0$ in such a case by inspection so that the formula (5.3) is also trivial. For one of the non-trivial cases, we have:



which agrees with the formula (5.3). The verification of the other patterns is similar. Thus the action of $r_{p,2}$ coincides with the cluster one. Then the statement for $r_{p,1}$ follows from Proposition 3.12 and Lemma 5.8. \blacksquare

Weyl group actions on $\mathcal{L}_{\mathfrak{sl}_3}^a(\Sigma, \mathbb{Q})$. The Weyl group actions on the bounded \mathfrak{sl}_3 -laminations are much easier to describe. Fix a puncture $p \in \mathbb{M}_o$, and let $W_p(u_1, u_2)$ denote the bounded \mathfrak{sl}_3 -lamination consisting of the peripheral component with counter-clockwise orientation of weight $u_1 \in \mathbb{Q}$, and the peripheral component with clockwise orientation of weight $u_2 \in \mathbb{Q}$. Then the reflections $r_{p,1}, r_{p,2}$ only transform the peripheral components around p as follows, and keep the other part intact:

$$\begin{aligned}
 r_{p,1} : W_p(u_1, u_2) &\mapsto W_p(-u_1, u_1 + u_2), \\
 r_{p,2} : W_p(u_1, u_2) &\mapsto W_p(u_1 + u_2, -u_2).
 \end{aligned} \tag{5.4}$$

Proposition 5.12. *The action map $H_{\mathcal{A}}(\mathbb{Q}^T) \rightarrow \mathcal{L}_{\mathfrak{sl}_3}^a(\Sigma, \mathbb{Q})$ in the cluster exact sequence (3.5) is equivariant under the action of $W(\mathfrak{sl}_3)^{\mathbb{M}_o}$. Moreover, the action of $W(\mathfrak{sl}_3)^{\mathbb{M}_o}$ on $\mathcal{L}_{\mathfrak{sl}_3}^a(\Sigma, \mathbb{Q})$ coincides with the cluster action.*

Proof. Observe that $W_p(u_1, u_2)$ is given by the coweight $u_1\varpi_1^\vee + u_2\varpi_2^\vee$ under the $H_{\mathcal{A}}(\mathbb{Q}^T)$ -action. Then the first statement can be verified by comparing the action (5.4) with the action of $W(\mathfrak{sl}_3)$ on the coweight lattice.

Given a rational bounded \mathfrak{sl}_3 -lamination $L \in \mathcal{L}_{\mathfrak{sl}_3}^a(\Sigma, \mathbb{Q})$ and $p \in \mathbb{M}_o$, let $u_{p,1}(L)$ (resp. $u_{p,2}(L)$) denote the total weight of the peripheral components in L around p with the counter-clockwise (resp. clockwise) orientation. Then for $s = 1, 2$, the PL function $-u_{p,s}(L)$ coincides with the max-plus tropicalization of the s -th partial potential [GS18, (203)] associated with the puncture p . In the labeled triangulation as in Figure 23, they are explicitly given by

$$\begin{aligned} u_{p,1}(L) &= \min\{a_3 + a_4 - a_1 - a_7, a_4 + a_5 - a_2 - a_8, a_5 + a_6 - a_2 - a_9, a_6 + a_3 - a_1 - a_{10}\}, \\ u_{p,2}(L) &= \min\{a_1 + a_2 - a_4, a_1 + a_2 - a_6\}, \end{aligned}$$

where $a_i := a_i^{\Delta(p)}(L)$ for $i = 1, \dots, 10$. By [GS18, Theorem 8.2], the cluster action is given by

$$\begin{aligned} (r_{p,1})_{\Delta(p)} : a_i &\mapsto \begin{cases} a_i - u_{p,1} & \text{if } i = 3, 4, 5, 6, \\ a_i & \text{otherwise,} \end{cases} \\ (r_{p,2})_{\Delta(p)} : a_i &\mapsto \begin{cases} a_i - u_{p,2} & \text{for } i = 1, 2, \\ a_i & \text{otherwise.} \end{cases} \end{aligned}$$

Then the cluster action transforms the functions $u_{p,s}$ as

$$\begin{aligned} u_{p,1}(r_{p,1}(L)) &= u_{p,1}(L) - 2u_{p,1}(L) = -u_{p,1}(L), \\ u_{p,2}(r_{p,1}(L)) &= u_{p,2}(L) + u_{p,1}(L), \\ u_{p,1}(r_{p,2}(L)) &= u_{p,1}(L) + u_{p,2}(L), \\ u_{p,2}(r_{p,2}(L)) &= u_{p,2}(L) - 2u_{p,2}(L) = -u_{p,2}(L). \end{aligned}$$

Comparing to (5.4), we see that this cluster action coincides with the geometric action. \blacksquare

Remark 5.13. As we mentioned in the above proof, the coefficients of the PL function $\mathbf{w}_p = u_{p,1}\varpi_1^\vee + u_{p,2}\varpi_2^\vee : \mathcal{L}_{\mathfrak{sl}_3}^a(\Sigma, \mathbb{Q}) \rightarrow \mathbb{Q}_{\mathbb{Q}}^\vee$ in the splitting (3.11) with respect to the \mathbb{Q} -basis $(\varpi_1^\vee, \varpi_2^\vee)$ are given by minus the tropicalized partial potentials. By a similar consideration, the coefficients of \mathbf{w}_m for any special point $m \in \mathbb{M}_\partial$ are also minus the tropicalized partial potentials introduced in [GS15, Section 2.1.4] (see also [GS19, Proposition 10.10]).

As an application of Theorem 5.11, let us briefly discuss an enhancement of [IK22, Theorem 1] on the equivariance statement.

Theorem 5.14. *The shear coordinate systems on $\mathcal{L}_{\mathfrak{sl}_3}^x(\Sigma, \mathbb{Q})$ give rise to an $(MC(\Sigma) \times \text{Out}(SL_3)) \ltimes W(\mathfrak{sl}_3)^{\mathbb{M}_0}$ -equivariant bijection*

$$\mathbf{x}_\bullet : \mathcal{L}_{\mathfrak{sl}_3}^x(\Sigma, \mathbb{Q}) \xrightarrow{\sim} \mathcal{X}_{PGL_3, \Sigma}(\mathbb{Q}^T). \quad (5.5)$$

Here the semi-direct product is induced from the action of $(\phi, *) \in MC(\Sigma) \times \text{Out}(SL_3)$ on $(w_p)_p \in W(\mathfrak{sl}_3)^{\mathbb{M}_0}$ defined by $(\phi, *).(w_p)_p := (w_{\phi(p)}^*)_p$.

Here the right-hand side is the same as $\mathcal{X}_{\mathfrak{sl}_3, \Sigma}^{\text{uf}}(\mathbb{Q}^T)$.

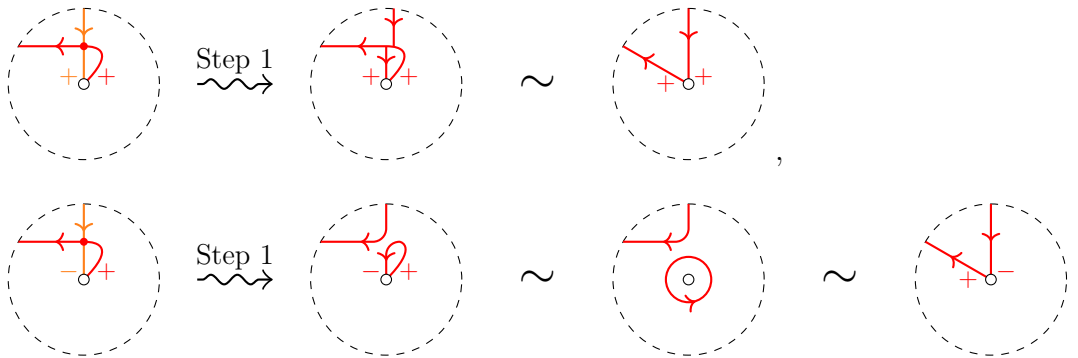
Proof. The statement that \mathbf{x}_\bullet is an $MC(\Sigma) \times \text{Out}(SL_3)$ -equivariant bijection is proved in [IK22]. It is also $W(\mathfrak{sl}_3)^{\mathbb{M}_0}$ -equivariant by Theorem 5.11. The actions of $MC(\Sigma) \times \text{Out}(SL_3)$ and $W(\mathfrak{sl}_3)^{\mathbb{M}_0}$ on $\mathcal{L}_{\mathfrak{sl}_3}^x(\Sigma, \mathbb{Q})$ combine together to an action of the semi-direct product by Lemma 5.8 and the local nature of the Weyl group actions around punctures. Alternatively, it is a consequence of the corresponding statement for the cluster action on $\mathcal{X}_{PGL_3, \Sigma}$ [GS18, Theorem 1.2]. \blacksquare

The statement is extended to that for $\mathcal{L}_{\mathfrak{sl}_3}^p(\Sigma, \mathbb{Q})$ and $\mathcal{P}_{PGL_3, \Sigma}(\mathbb{Q}^T) = \mathcal{X}_{\mathfrak{sl}_3, \Sigma}(\mathbb{Q}^T)$ in an obvious manner (cf. [IK22, Theorem 2]).

5.3. Proofs of the statements in Section 5. We first give a proof of Lemma 5.5, and then proceed to the proof of Proposition 5.4.

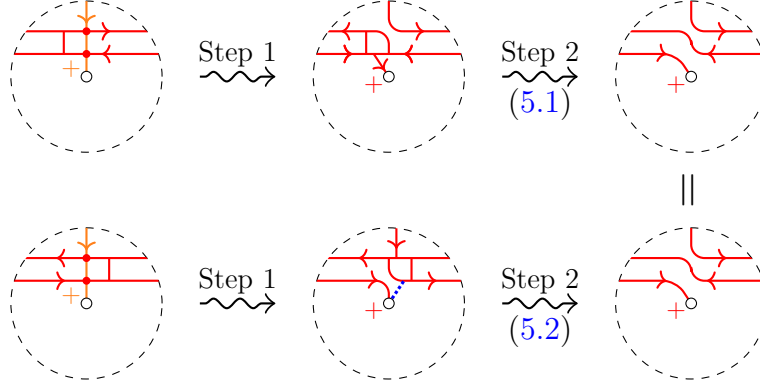
Proof of Lemma 5.5. The proof is a straightforward case-by-case verification. We illustrate it by showing a couple of examples.

(1): In the first move, we need to consider the four possible patterns of the orientation/sign of the orange end. We have:



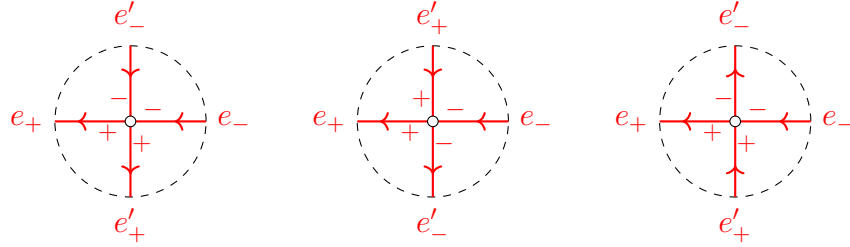
Here we have used the moves (E3) and (E4), and the reverse resolution procedure in the second case. Verification for the other two patterns is left to the reader. The verification of the second move is similar.

(2): In the first move, we have:

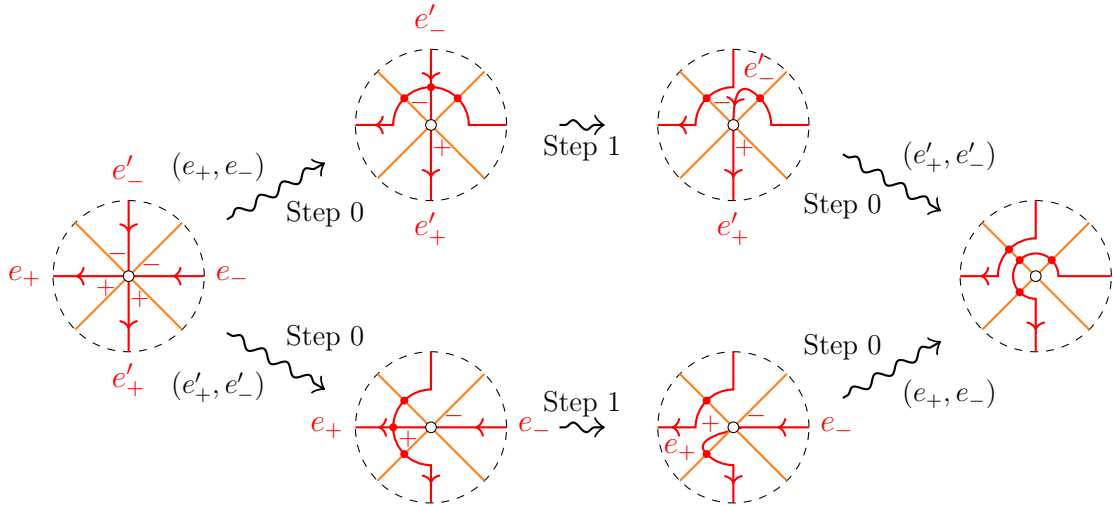


Similarly for the other three patterns of the orange end. ■

Proof of Proposition 5.4. (1): It is clear that the resolution operations at different punctures commute. Consider two resolvable pairs (e_+, e_-) , (e'_+, e'_-) at a common puncture $p \in \mathbb{M}_o$. If the ends e_+, e_-, e'_+, e'_- are located in this order clockwise, then their resolutions do not intersect and thus the resolution operations commute. Up to symmetry, we need to consider the following three patterns of their clockwise ordering:

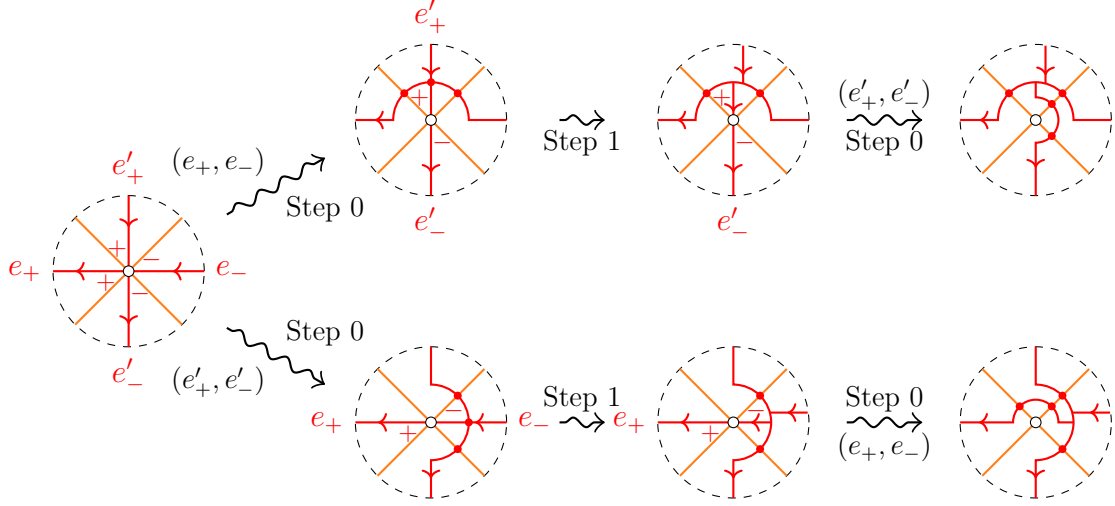


The associativity for the first configuration is verified as follows:

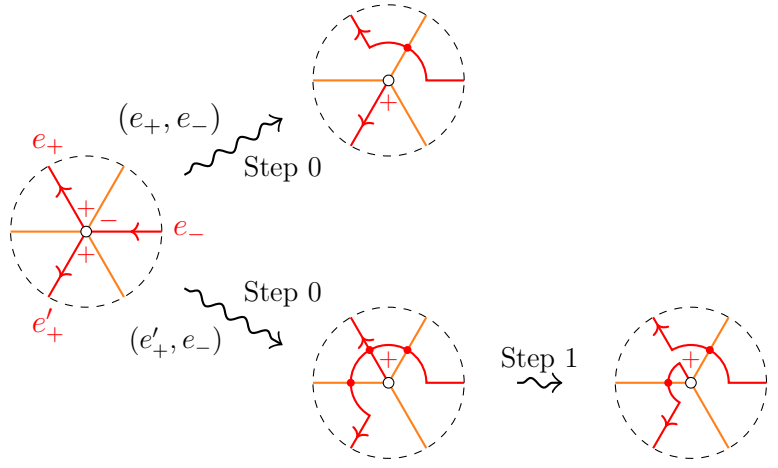


Here the other ends incident to p are shown in orange, whose orientations do not matter. The resulting generalized signed webs in the two routes are equivalent. The second

configuration gives rise to:



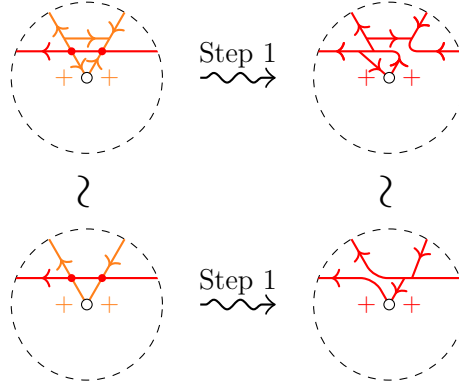
Then the equivalence of the resulting generalized signed webs follows from Lemma 5.5 (2). The third pattern coincides with the second one by turning it upside-down. Thus the first statement is proved. The case $e'_- = e_-$ in the second statement is verified as



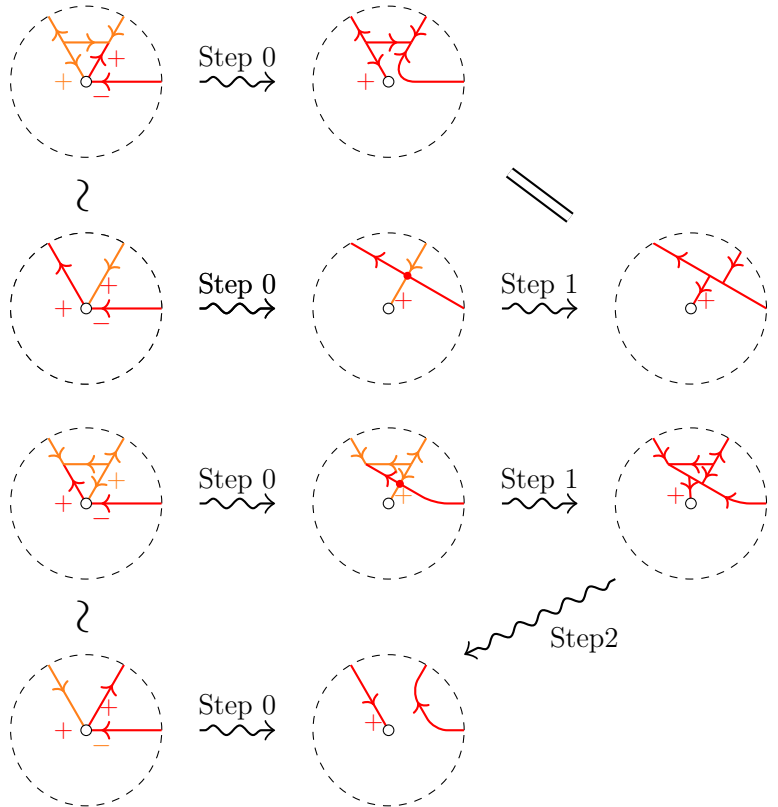
where the equivalence of the resulting generalized signed webs follows from Lemma 5.5 (1). The case $e'_+ = e_+$ is similar.

(2): The resolution operations clearly commute with the elementary moves (E1) and (E2), since they do not affect the punctures. We do not need to care about (E4), since it cannot be applied in the presence of a resolvable pair. It remains to prove the compatibility with the puncture H-moves (E3). For the first move (3.6), when the resolvable pair is not

contained in the ends involved in (3.6), we have



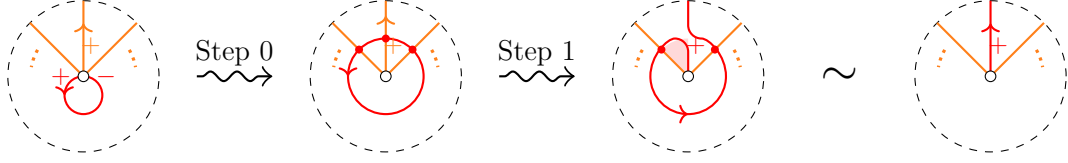
The verification for the other possible orientations/signs is similar. Indeed, it is the common situation for these cases that one intersection point is smoothly resolved, while the other one is resolved with extra trivalent vertices. When the resolvable pair is involved, we have



The verification for the other possible orientations/signs is similar. The compatibility with the second move (3.7) can be similarly verified, which is left to the reader. ■

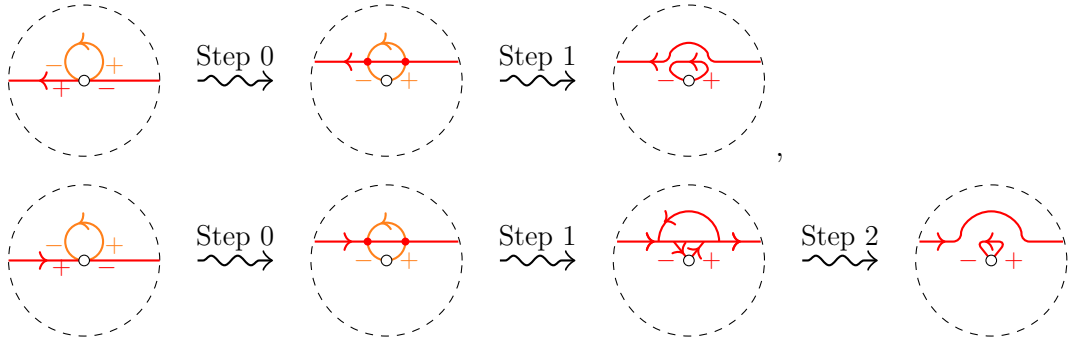
Proof of Lemma 5.6. If there are no other ends incident to the puncture p , then we can remove C by (E4) after the resolution process (Step 0). Assume that W has at least one

end incident to p that is outgoing with positive sign. Then we have:

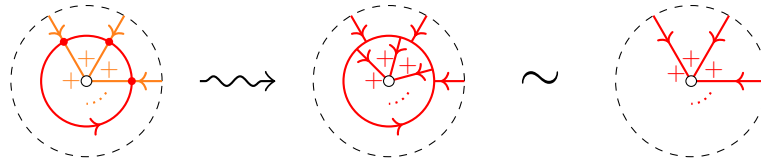


Here in the last step, we applied Lemma 5.5 (1) successively. After all, the result is the same as just removing the component C . Similarly for the case where W has at least one other incoming end with negative sign.

Then we need to consider the case where W has only other ends which are incoming with positive signs and outgoing with negative signs. Choose arbitrary resolvable pairs among them. If the resolution direction is the opposite to C (namely, the component C lies in the lower-half plane in the situation of Step 1 in Definition 5.1), then we can simply resolve them without touching C . Otherwise, we have:



Here in the second case, observe that we have used the 4-gon elimination rule (5.1) arising from a 3-gon face. In each case, the result is the same as just resolving the pair without touching C . In these ways, we can at once move all possible resolvable pairs away from p . The remaining ends are either all incoming with positive signs or all outgoing with negative signs. Therefore we can remove C by using (E4), as follows:



Finally, we restore the resolvable pairs to get the original diagram except for the component C removed. The assertion is proved. \blacksquare

6. RELATION TO THE WORK OF SHEN–SUN–WENG

Here we briefly explain the relation to the \mathcal{X} -webs considered in the recent work of Shen–Sun–Weng, and give a proof of [SSW23, Conjecture 4.10]. This correspondence may be also useful to recognize a reasonable subset of the space $\mathcal{L}_{\mathfrak{sl}_3}^p(\Sigma, \mathbb{Z})$ introduced in [IK22].

Recall from [IK22, Section 4] the space

$$\mathcal{L}_{\mathfrak{sl}_3}^p(\Sigma, \mathbb{Z}) := \mathcal{L}_{\mathfrak{sl}_3}^x(\Sigma, \mathbb{Z}) \times (\mathbb{P}^\vee)^\mathbb{B}$$

of rational \mathcal{P} -laminations. It consists of the pairs (\widehat{L}, ν) of $\widehat{L} \in \mathcal{L}_{\mathfrak{sl}_3}^x(\Sigma, \mathbb{Z})$ and $\nu = (\nu_E)_{E \in \mathbb{B}}$, where $\nu_E = \nu_E^+ \varpi_1^\vee + \nu_E^- \varpi_2^\vee \in \mathbb{P}^\vee$ is called the *pinning* assigned to the boundary interval $E \in \mathbb{B}$.

We say that a coweight $\lambda \in \mathbb{P}^\vee$ is *dominant* (resp. *anti-dominant*) if $\lambda \in \mathbb{P}_+^\vee := \mathbb{Z}_+ \varpi_1^\vee + \mathbb{Z}_+ \varpi_2^\vee$ (resp. $-\lambda \in \mathbb{P}_+^\vee$). For each $p \in \mathbb{M}_o$, let

$$\theta_p : \mathcal{L}_{\mathfrak{sl}_3}^p(\Sigma, \mathbb{Z}) \rightarrow \mathcal{L}_{\mathfrak{sl}_3}^x(\Sigma, \mathbb{Z}) \rightarrow \mathbb{P}^\vee$$

be the tropicalized Casimir map. Here the first map forgets the pinnings.

Definition 6.1. Let $\mathcal{L}_{\mathfrak{sl}_3}^p(\Sigma, \mathbb{Z})_0 \subset \mathcal{L}_{\mathfrak{sl}_3}^p(\Sigma, \mathbb{Z})$ be the subset consisting of (\widehat{L}, ν) such that

- (1) For each $p \in \mathbb{M}_o$, the value $\theta_p(\widehat{L}, \nu) \in \mathbb{P}^\vee$ is dominant.
- (2) For each $E \in \mathbb{B}$, the pinning $\nu_E \in \mathbb{P}^\vee$ is anti-dominant.

Lemma 6.2. *We have a natural bijection*

$$\mathcal{L}_{\mathfrak{sl}_3}^p(\Sigma, \mathbb{Z})_0 \xrightarrow{\sim} \mathcal{W}_\Sigma^\mathcal{X},$$

where the right-hand side denotes the set of “ \mathcal{X} -webs” in [SSW23, Definition 2.6].

Proof. The correspondence is as follows. Let $(\widehat{L}, \nu) \in \mathcal{L}_{\mathfrak{sl}_3}^p(\Sigma, \mathbb{Z})$, and represent \widehat{L} by a non-elliptic reduced signed web W with weight 1 on each component.

- From the defining rule of θ_p in Figure 2, the dominant condition for θ_p requires W to have + sign at each end at punctures. We identify an end of + sign with an end without signs.
- We shift each end of W at a boundary interval in the positive direction along $\partial\Sigma$ until it hits a special point.
- In view of the correspondence \tilde{p} given in [IK22, Section 4.3], we identify the anti-dominant pinning assigned to $E \in \mathbb{B}$ with the peripheral components around the initial special point of E .

Thus we identify W with a reduced web with ends only at \mathbb{M} , and the anti-dominant pinnings equip W with peripheral components around \mathbb{M}_∂ . It is easily checked that the topological conditions for the \mathcal{X} -webs match up with our non-elliptic and reduced conditions. ■

Lemma 6.3. *The canonical bijection (5.5) induces*

$$\mathcal{L}_{\mathfrak{sl}_3}^p(\Sigma, \mathbb{Z})_0 \xrightarrow{\sim} \mathcal{P}_{PGL_3, \Sigma}^+(\mathbb{Z}^T),$$

where $\mathcal{P}_{PGL_3, \Sigma}^+(\mathbb{Z}^T) \subset \mathcal{P}_{PGL_3, \Sigma}(\mathbb{Z}^T)$ is the subspace introduced in [SSW23, Section 4.3.A].

Proof. Recall that $\mathcal{P}_{PGL_3, \Sigma}^+(\mathbb{Z}^T)$ is defined by (1) the dominance condition for the monodromy around each puncture, and (2) the negative condition for the tropicalized potential around each special point. Let us examine these conditions.

(1): For each puncture $p \in \mathbb{M}_o$, let $\Theta_p : \mathcal{P}_{PGL_3, \Sigma} \rightarrow H$ be the positive map that takes the semi-simple part of the monodromy of a PGL_3 -local system around p with respect to its framing. Proposition 4.4 means that θ_p coincides with the tropicalization $\Theta_p^T : \mathcal{P}_{PGL_3, \Sigma}(\mathbb{Z}^T) \rightarrow H(\mathbb{Z}^T) = \mathbb{P}^\vee$. Then their condition $\Theta_p^T \in \mathbb{P}_+^\vee$ is nothing but our condition $\theta_p \in \mathbb{P}_+^\vee$.

(2): For a special point $m \in \mathbb{M}_\partial$, let $P_m : \mathcal{A}_{SL_3, \Sigma} \rightarrow \mathbb{C}$ denote the total potential associated with m [SSW23, Section 4.1]. It descends to a potential function $W_m : \mathcal{P}_{PGL_3, \Sigma} \rightarrow \mathbb{C}$ such that

$$\begin{array}{ccc} \mathcal{A}_{SL_3, \Sigma} & \xrightarrow{P_m} & \mathbb{C}, \\ p \downarrow & \nearrow W_m & \\ \mathcal{P}_{PGL_3, \Sigma} & & \end{array}$$

where $\tilde{p} : \mathcal{A}_{SL_3, \Sigma} \rightarrow \mathcal{P}_{PGL_3, \Sigma}$ denotes the extended ensemble map. Choose an ideal triangulation Δ so that m belongs to exactly one triangle T . In the vertex labeling of the quiver on T as in Figure 14, the coordinate expressions of the potential functions P_m and W_m are

$$P_m = \frac{A_4}{A_1 A_2} + \frac{A_1 A_6}{A_3 A_4} + \frac{A_2 A_7}{A_4 A_5}, \quad W_m = X_1 + X_3(1 + X_4).$$

The tropicalization of the latter gives

$$W_m^T = \mathbf{w}_m = \max\{\mathbf{x}_1, \mathbf{x}_3 + [\mathbf{x}_4]_+\}.$$

Therefore the condition $W_m^T \leq 0$ is equivalent to

$$\nu_E^+ = \mathbf{x}_1 \leq 0, \quad \nu_E^- = \mathbf{x}_3 + [\mathbf{x}_4]_+ \leq 0.$$

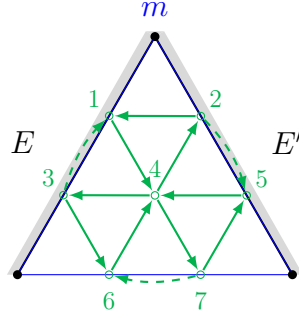
Here recall the formula [IK22, (4.3)], with a notice that $\alpha_E^\pm(\widehat{L}) = 0$ from our choice of Δ . Thus $W_m^T \leq 0$ is equivalent to $-\nu_E \in \mathbb{P}_+^\vee$.

Hence these conditions are equivalent to (1) and (2) in Definition 6.1, respectively. The assertion is proved. \blacksquare

Remark 6.4. As we have noted in Remark 5.13, $\mathbf{w}_m = -P_m^T$ counts the total weight of the peripheral components around $m \in \mathbb{M}_\partial$. The computation above is in accordance with the extended geometric ensemble map $\tilde{p} : \mathcal{L}_{\mathfrak{sl}_3}^a(\Sigma, \mathbb{Q}) \rightarrow \mathcal{L}_{\mathfrak{sl}_3}^p(\Sigma, \mathbb{Q})$ [IK22, Section 4.3] which relates the pinnings with minus the peripheral weights.

Combining Lemmas 6.2 and 6.3, we get:

Corollary 6.5 ([SSW23, Conjecture 4.10]). $\mathcal{W}_\Sigma^{\mathcal{X}} \cong \mathcal{P}_{PGL_3, \Sigma}^+(\mathbb{Z}^T)$.

FIGURE 14. The quiver around a special point m .

Remark 6.6. Here is a remark on the ‘anti’-dominant condition in Definition 6.1. If we use the *Langlands dual shear coordinates* \check{x}_i [IK22, Section 4] (which are related to the shear coordinates by a quasi-cluster transformation), we can convert it to the dominant condition in the following sense.

Let us consider the potential function $\check{W}_m : \mathcal{P}_{PGL_3, \Sigma} \rightarrow \mathbb{C}$ satisfying

$$\begin{array}{ccc} \mathcal{A}_{SL_3, \Sigma} & \xrightarrow{P_m} & \mathbb{C}, \\ \check{p} \downarrow & \nearrow \check{W}_m & \\ \mathcal{P}_{PGL_3, \Sigma} & & \end{array}$$

where $\check{p} : \mathcal{A}_{SL_3, \Sigma} \rightarrow \mathcal{P}_{PGL_3, \Sigma}$ assigning the pinning $(A_E^-, \pi(A_E^+))$ to each boundary interval $E \in \mathbb{B}$. Here A_E^+, A_E^- stands for the SL_3/U^+ -decoration assigned to the initial and terminal point of E , respectively, and the map π takes the underlying flag. Given an ideal triangulation Δ of Σ , recall from [IK22, Section 5] that the Langlands dual coordinates \check{x}_i^Δ are defined by $\check{x}_i^\Delta := x_i^\Delta$ for $i \in I_{\text{uf}}(\Delta)$, and by modifying the frozen coordinates on $E \in \mathbb{B}$ by

$$\begin{aligned} \check{x}_{E,1}^\Delta(\widehat{L}, \nu) &:= \nu_E^+ + \check{\alpha}_E^+(\widehat{L}) + [-x_T(\widehat{L})]_+,^1 \\ \check{x}_{E,2}^\Delta(\widehat{L}, \nu) &:= \nu_E^- + \check{\alpha}_E^-(\widehat{L}). \end{aligned}$$

Here T is the unique triangle having E as an edge; $\check{\alpha}_E^+(\widehat{L})$ (resp. $\check{\alpha}_E^-(\widehat{L})$) is the total weight of the oriented corner arcs in $\mathcal{W} \cap T$ bounding the terminal endpoint of E in the counter-clockwise (resp. clockwise) direction.² In the Langlands dual coordinates, we have

$$\check{W}_m^T = \max\{-\check{x}_6, -\check{x}_5 + [-\check{x}_0]_+\} = -\min\{\check{x}_6, \check{x}_5 - [-\check{x}_0]_+\}.$$

¹See the third version on arXiv, where the third term is corrected from the published version [IK22, Section 5]. The assertions in [IK22, Proposition 5.3, Lemma 5.4] hold true only after this correction.

²We can also introduce the Langlands dual coordinates on the level of $\mathcal{P}_{PGL_3, \Sigma}$ by modifying the frozen coordinates on E by referring to the pinning $(A_E^-, \pi(A_E^+))$ instead of $(A_E^+, \pi(A_E^-))$.

Therefore the condition $\check{W}_m^T \leq 0$ is equivalent to $\nu_{E',2} = \check{x}_6 \geq 0$, $\nu_{E',1} = \check{x}_5 - [-\check{x}_0]_+ \geq 0$, namely $\nu_{E'} \in \mathbf{P}_+^\vee$.

Thus we could use the subspace $\mathcal{L}_{\mathfrak{sl}_3}^p(\Sigma, \mathbb{Z})_+$ such that $\theta_p(\widehat{L}, \nu) \in \mathbf{P}_+^\vee$ and $\nu_E \in \mathbf{P}_+^\vee$, which is identified with the subspace of $\mathcal{P}_{PGL_3, \Sigma}(\mathbb{Z}^T)$ cut out by the dominance condition for the monodromy and $\check{W}_m^T \leq 0$. It is a natural generalization of the subspace used in [IK22, Section 5], which corresponds to the graphical basis of the skein algebra when $\mathbb{M}_\circ = \emptyset$, and nicely fits in with the coordinate axiom of the quantum duality map via the Langlands dual coordinates.

A technical but important remark is that we should use the Langlands dual ensemble map \check{p} on the tropical side if we use the original ensemble map p on the function side (and vice versa) to fully satisfy the coordinate axioms on the extremal terms of quantum duality maps on the both sides.

7. RELATION TO THE WORK OF FRASER–PYLYAVSKYY

Here we indicate some relations between our formulation of unbounded \mathfrak{sl}_3 -laminations and the related work of Fraser–Pylyavskyy [FP21]. In what follows, we use the identification $\mathbf{P} \cong \mathbf{P}^\vee$, $\varpi_s = \varpi_s^\vee$ via the normalized Killing form of \mathfrak{sl}_3 .

7.1. Relation with the pseudo-tagged diagrams. Our integral unbounded \mathfrak{sl}_3 -laminations are related to *pseudo-tagged diagrams* of Fraser–Pylyavskyy, as follows. Here is the \mathfrak{sl}_3 -case of [FP21, Definition 8.11]:

Definition 7.1. A *pseudo-tagged \mathfrak{sl}_3 -diagram* is a web W on Σ together with a subset $\varphi(e) \subset \{1, 2, 3\}$ assigned to each end e of W incident to a puncture $p \in \mathbb{M}_\circ$. Here we impose

$$|\varphi(e)| = \begin{cases} 1 & \text{if } e \text{ is outgoing from } p, \\ 2 & \text{if } e \text{ is incoming to } p. \end{cases}$$

Here is a representation-theoretic meaning of the data $\varphi(e)$. Recall that the weight lattice of \mathfrak{sl}_3 is realized as

$$\mathbf{P} = \mathbb{Z}^3 / \langle \mathbf{e}_1 + \mathbf{e}_2 + \mathbf{e}_3 \rangle_{\mathbb{Z}},$$

where $(\mathbf{e}_1, \mathbf{e}_2, \mathbf{e}_3)$ denotes the standard basis of \mathbb{Z}^3 . Then for a subset $A \subset \{1, 2, 3\}$, we associate the vector $\iota_A := \sum_{i \in A} \mathbf{e}_i \in \mathbf{P}$. Recall the fundamental weights $\varpi_1 = \mathbf{e}_1$, $\varpi_2 = \mathbf{e}_1 + \mathbf{e}_2 \in \mathbf{P}$. Then we should have a correspondence so that the weight vector $\iota_{\varphi(e)} \in \mathbf{P}$ agrees with the contribution of e to the tropicalized Casimir function θ_p (Figure 2) of the end e . The correspondence is shown in Figure 15.

To each pseudo-tagged diagram (W, φ) , Fraser–Pylyavskyy associated a rational function $[W, \varphi] \in \mathcal{K}(\mathcal{A}_{SL_3, \Sigma})$ on the moduli space $\mathcal{A}_{SL_3, \Sigma}$ of decorated SL_3 -local systems on Σ [FP21, Definition 8.12]. They describe certain linear relations among these rational functions in their *flattening theorem*, whose concrete form is given in [FP21, Lemma 9.4].

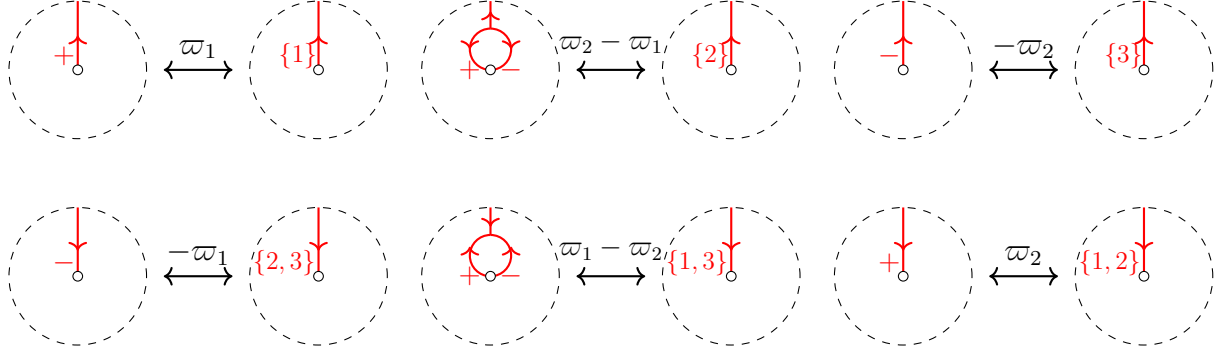


FIGURE 15. Correspondence between the sign (Left) and the tag (Right) of Fraser–Pylyavskyy. The value of the tropicalized Casimir is shown above the arrow.

We are going to discuss a relation between the formulae given there and our resolution move (Definition 5.1). We use the notation in [FP21, Section 9].

In the \mathfrak{sl}_3 -case, the non-trivial relations (in which the Grassmannian permutations w_S are non-trivial) are the following:

- $(a, b, c) = (0, 1, 1)$: $S = \{2\}$, $w_S = (1\ 2)$, and

$$\begin{array}{c} \{2\} \\ \diagup \\ \circ \\ \diagdown \\ \{1\} \end{array} = - \begin{array}{c} \{1, 2\} \\ \diagup \\ \circ \\ \diagdown \\ \{1, 2\} \end{array} + \begin{array}{c} \{1, 2\} \\ \diagup \\ \circ \\ \diagdown \\ \{1, 2\} \end{array}$$

- $(a, b, c) = (1, 1, 1)$: $S = \{1, 3\}$, $w_S = (2\ 3)$, and

$$\begin{array}{c} \{1, 2\} \\ \diagup \\ \circ \\ \diagdown \\ \{1, 3\} \end{array} = - \begin{array}{c} \{1\} \\ \diagup \\ \circ \\ \diagdown \\ \{1\} \end{array} + \begin{array}{c} \{1\} \\ \diagup \\ \circ \\ \diagdown \\ \{1\} \end{array}$$

- $(a, b, c) = (0, 2, 1)$: $S = \{3\}$, $w_S = (1\ 3)$, and

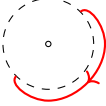
$$\begin{array}{c} \{1, 2\} \\ \diagup \\ \circ \\ \diagdown \\ \{3\} \end{array} = \begin{array}{c} \circ \\ \diagup \\ \diagdown \end{array} - 2 \begin{array}{c} \circ \\ \diagup \\ \diagdown \end{array} + \begin{array}{c} \circ \\ \diagup \\ \diagdown \end{array} \\ = \begin{array}{c} \circ \\ \diagup \\ \diagdown \end{array} + \begin{array}{c} \circ \\ \diagup \\ \diagdown \end{array} + \begin{array}{c} \circ \\ \diagup \\ \diagdown \end{array}.$$

Here the right-hand side is computed using the \mathfrak{sl}_3 -skein relation.

- $(a, b, c) = (0, 1, 2)$: $S = \{2, 3\}$, $w_S = (1\ 2)(2\ 3)$, and

$$\begin{aligned}
 \text{Diagram 1} &= \text{Diagram 2} - 2 \text{Diagram 3} + \text{Diagram 4} \\
 &= \text{Diagram 5} + \text{Diagram 6} + \text{Diagram 7}
 \end{aligned}$$

Here the computation is similar to the previous case.

By connecting  to the both sides in the first two cases and appropriately rotating the latter two cases, we get the following relations:

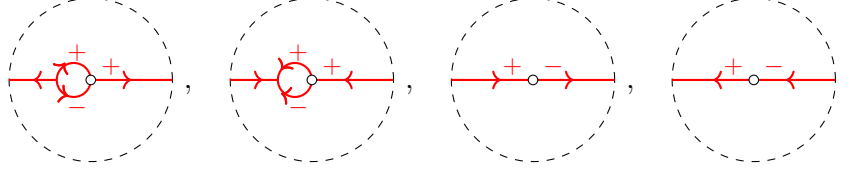
$$\text{Diagram 1} = \text{Diagram 2} + \text{Diagram 3} \tag{7.1}$$

$$\text{Diagram 1} = \text{Diagram 2} + \text{Diagram 3} \tag{7.2}$$

$$\text{Diagram 1} = \text{Diagram 2} + \text{Diagram 3} + \text{Diagram 4} \tag{7.3}$$

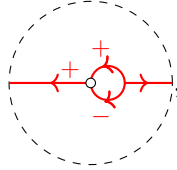
$$\text{Diagram 1} = \text{Diagram 2} + \text{Diagram 3} + \text{Diagram 4} \tag{7.4}$$

We remark here that the right-hand sides of (7.1)–(7.4) coincide with (the classical limit of) the higher-rank analogue of the *Roger–Yang skein relations* [RY14] found by Shen–Sun–Weng and systematically studied in their upcoming work [SSW].³ From the correspondence given in Figure 15, the left-hand sides of (7.1)–(7.4) correspond to

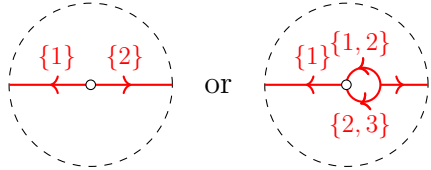


respectively. Then we see that after applying the resolution move (Definition 5.1) to them, they give rise to one of the terms in the right-hand sides. Therefore our approach seems to be consistent with the Fraser–Pylyavskyy’s work, under the belief that our \mathfrak{sl}_3 -laminations should parametrize the “highest (or lowest) terms” of web functions on $\mathcal{A}_{SL_3, \Sigma}$ in some sense. The justification of this point will require further research.

Remark 7.2. While we have the basic correspondence between our signed webs and the pseudo-tagged diagrams of Fraser–Pylyavskyy, we still need care to obtain a well-defined map between them. For example, the signed web



may be viewed as either of the pseudo-tagged diagrams



according to the rule shown in Figure 15. It seems that the first one is appropriate. Indeed, one can show that the second one is zero using the relation (7.4) and the usual \mathfrak{sl}_3 -skein relations. See [FP21, Remark 8.16] for a seemingly related remark. We do not pursue this point here.

7.2. Relation with the dosps. In [FP21, Sections 5–7], they formulate a higher rank analogue of *tagged triangulations* used in the \mathfrak{sl}_2 -case ([FST08]) to describe certain seeds obtained by mutating those associated with the usual ideal triangulations of Σ . Their idea is as follows.

³T. I. first learned their \mathfrak{sl}_3 -version of Roger–Yang relations corresponding to (7.3), (7.4) from Zhe Sun. Those corresponding to (7.1), (7.2) have been found independently by T.I. and Wataru Yuasa, and Shen–Sun–Weng.

They firstly consider the weights of cluster variables with respect to the H -action on $\mathcal{A}_{SL_3, \Sigma}$ associated with each puncture p . They formulated a certain compatibility condition on a collection of H -weights, and conjectured that the collection of H -weights of any cluster should be compatible [FP21, Conjecture 5.4]. Such a compatible collection of H -weights gives rise to a *decorated ordered set partition* (abbreviated as “dosp”) [FP21, Definition 6.6], which is a choice of a Weyl region (*i.e.*, a facet in the Coxeter complex) together with some decoration by signs. The dosps give a higher rank analogue of tags. Then [FP21, Theorem 7.3] describes the projection from the “good part” of the exchange graph to the graph of dosps (whose edges are given by *dosp mutations*) at each puncture. Summarizing, each cluster in $\mathcal{A}_{SL_3, \Sigma}$ is (conjecturally) colored by dosps at punctures, and the seed mutations induce dosp mutations.

Now we are going to relate our construction to this theory. Extending the conjectures by Fomin–Pylyavskyy [FP14, FP16], Fraser–Pylyavskyy give conjectures [FP21, Section 8.5] that each cluster is represented by a certain collection of pseudo-tagged diagrams. We then expect that such a collection corresponds to a collection of signed webs.

Definition 7.3. The *lamination cluster* associated to $v \in \mathbb{Exch}_{\mathfrak{sl}_3, \Sigma}$ is the collection $\{W_j\}_{j \in I_{\text{uf}}}$ of signed webs on Σ satisfying $x_i^{(v)}(W_j) = \delta_{ij}$ for $i, j \in I_{\text{uf}}$.

In particular, each lamination cluster $\{W_j\}_{j \in I_{\text{uf}}}$ gives rise to a P -cluster $\{\theta_p(W_j)^*\}_{j \in I_{\text{uf}}} \subset \mathbf{P}$ in the sense of [FP21], which determines a dosp.

Let us consider the punctured disk D^* with two special points. Recall the classification of spiralling diagrams in Proposition 4.2. In this case, their conjectures are shown to be true [FP21, Proposition 10.3]. Following the proof of [FP21, Theorem 7.3], we first move on to the cluster that gives the initial seed in the corresponding *Grassmannian moduli space* \mathcal{A}'_{SL_3, D^*} [FP21, Definition 3.3] (cluster type D_4), up to the deletion of cluster variables with zero weight. The mutation sequence starting from our initial cluster is shown in Figure 16.

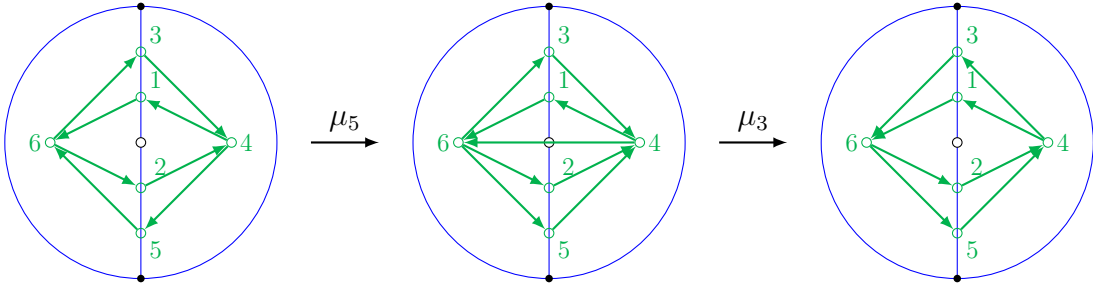


FIGURE 16. Transformation from the initial seed in \mathcal{A}_{SL_3, D^*} to the initial seed in the Grassmannian moduli space \mathcal{A}'_{SL_3, D^*} .

Deleting the vertices 3, 5 in the right-most picture in Figure 16, we get the initial quiver in [FP21, Example 5.7]. The corresponding sequence of lamination clusters is shown in Figure 17. Observe that the signed webs associated to the vertices 3, 5 in the right-most

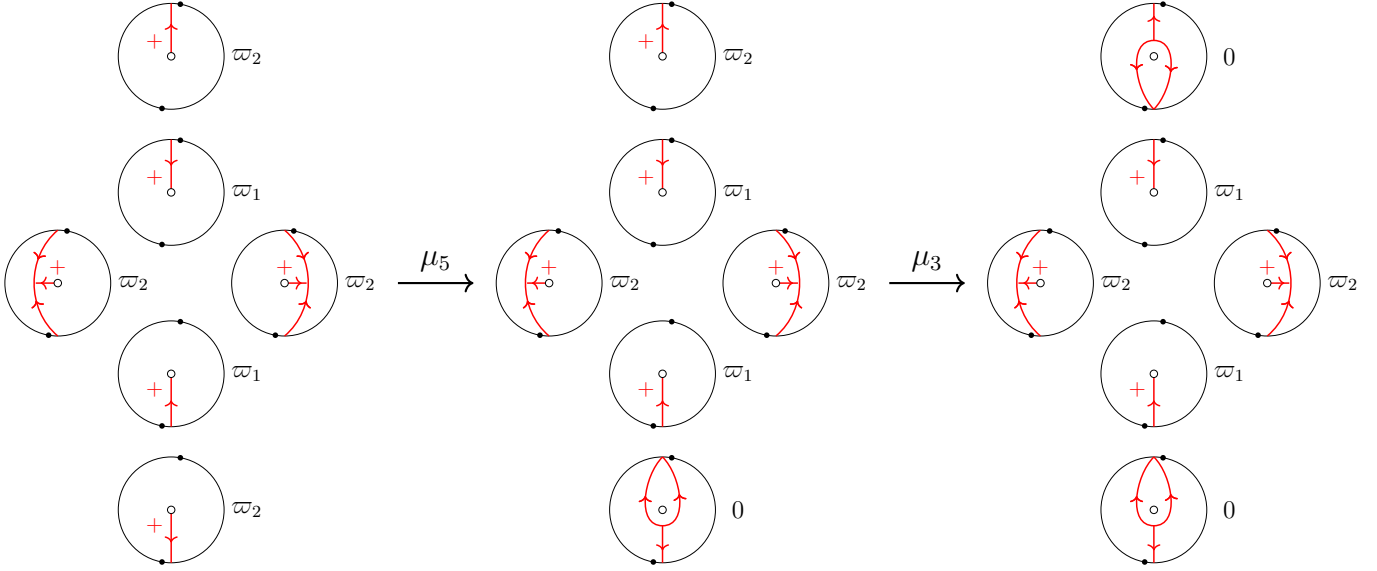


FIGURE 17. Transformation of the lamination clusters corresponding to Figure 16. Here the values of θ_p^* are indicated. During the process, the associated dosp is $1|2|3$.

picture have $\theta_p^* = 0$, and thus do not contribute to the dosp at p . During this sequence, the associated dosp is $1|2|3$ (dominant chamber).

Then one can walk around the exchange graph of type D_4 (freezing the vertices 3, 5) to get all the dosp following the algorithm illustrated in [FP21, Example 7.7 and Lemma 7.8]. See also [FP21, Figure 2]. For example, the dosp mutation $1|2|3 \rightarrow 12|3 \rightarrow 123^+$ are shown in Figures 18 and 19, respectively.

8. A BRIEF DISCUSSION ON HIGHER RANK GENERALIZATIONS

Here we propose a possible direction of higher rank generalizations of our formulation of unbounded laminations. See also the first arXiv version of [Kim21].

We propose to use the approach of [MOY98] and [CKM14]. For a complex semisimple Lie algebra \mathfrak{g} , a \mathfrak{g} -web on Σ is an immersed oriented uni-trivalent graph W on Σ , where each edge is colored by a vertex $s \in S$ of the Dynkin diagram of \mathfrak{g} , corresponding to the s -th fundamental weight ϖ_s . The boundary condition on the univalent vertices is the same as in the \mathfrak{sl}_3 -case. At each trivalent vertex, the colors (s, t, u) are required to satisfy the condition

$$\dim_{\mathbb{C}}(V(\varpi_s) \otimes V(\varpi_t) \otimes V(\varpi_u))^G = 1,$$

where $V(\lambda)$ denotes the irreducible representation with the highest weight λ .

A signed \mathfrak{g} -web is a \mathfrak{g} -web together with a sign (+ or -) assigned to each end incident to a puncture. Then a rational unbounded \mathfrak{g} -laminations should be defined as a certain

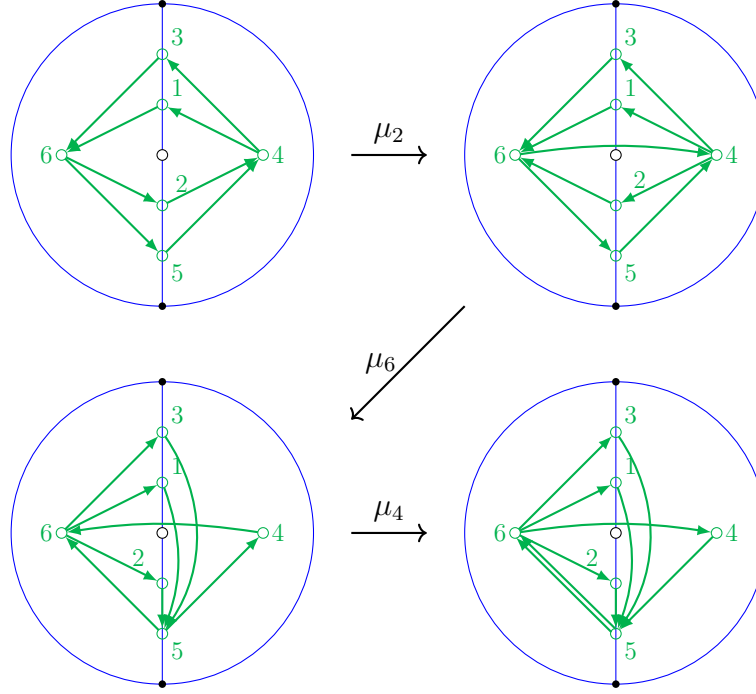


FIGURE 18. Mutation sequence that realizes the dosp mutation $1|2|3 \rightarrow 12|3 \rightarrow 123^+$.

equivalence class of a signed \mathfrak{g} -web equipped with rational weights on its components. A correct description of equivalence relations as given in Section 3 will require additional elaboration in the higher rank cases. Assume that the space $\mathcal{L}_{\mathfrak{g}}^x(\Sigma, \mathbb{Q})$ of rational unbounded \mathfrak{g} -lamination on Σ is appropriately defined.

For each puncture $p \in \mathbb{M}_o$, we should have the tropicalized Casimir map

$$\theta_p : \mathcal{L}_{\mathfrak{g}}^x(\Sigma, \mathbb{Q}) \rightarrow \mathbb{P}_{\mathbb{Q}}^{\vee}.$$

The contribution of each signed end to θ_p should be as shown in Figure 20. Here $* : S \rightarrow S$, $s \mapsto s^*$ is the Dynkin involution defined by $w_0 \varpi_s = -\varpi_{s^*}$, where $w_0 \in W(\mathfrak{g})$ is the longest element of the Weyl group.

Observe that the data of signs and the fundamental weights are enough for the values of θ_p to exhaust the coweight lattice \mathbb{P}^{\vee} , so we expect no additional data assigned to the ends.

Recall the construction of cluster variables $\Delta_{\lambda, \mu, \nu}$ on $\mathcal{A}_{G^{\vee}, \Sigma}$ from [GS19, Section 9]. Here G^{\vee} is the simply-connected group with the Langlands dual Lie algebra \mathfrak{g}^{\vee} . In particular, they are determined by the triple (λ, μ, ν) of weights for \mathfrak{g}^{\vee} (=coweights for \mathfrak{g}) up to a scalar. Based on the quantum duality conjecture [FG09], the \mathfrak{g} -webs W should correspond to functions F_W on $\mathcal{A}_{G^{\vee}, \Sigma}$ in a similar manner as in [IK23, IK22], at least when $\mathbb{M}_o = \emptyset$. Some of the \mathfrak{g} -webs corresponding to cluster variables on the dual side are shown in Figure 21, together with the \mathfrak{g}^{\vee} -weights (= \mathfrak{g} -coweights) of the cluster variables.

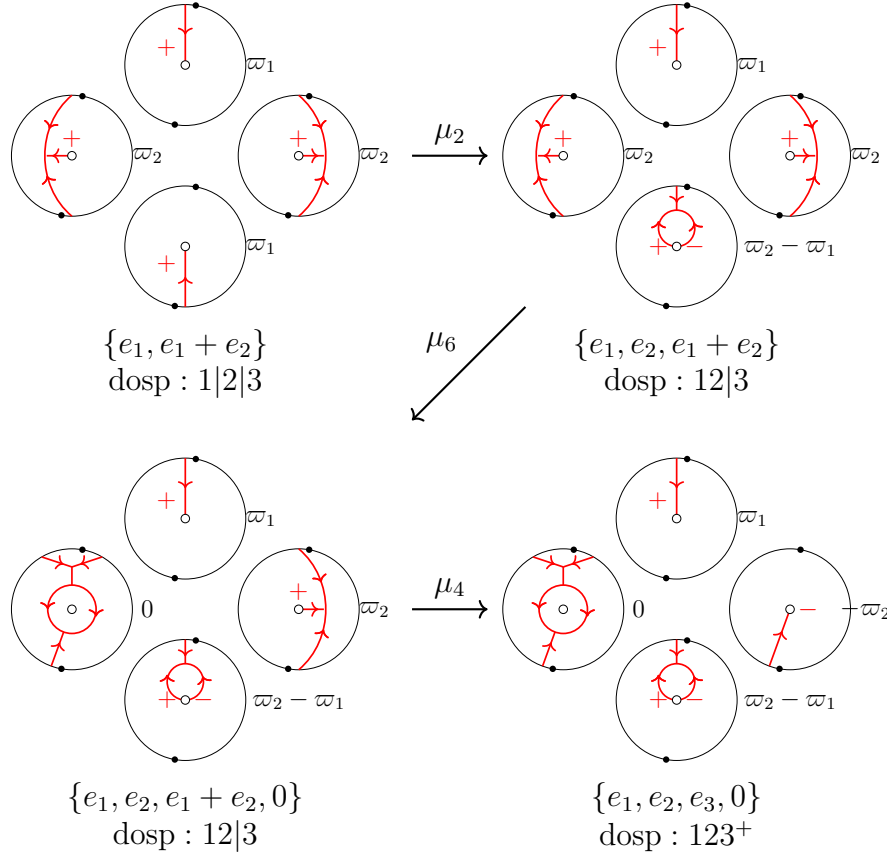


FIGURE 19. The sequence of lamination clusters corresponding to Figure 18. The associated P -clusters and the dops are also shown.

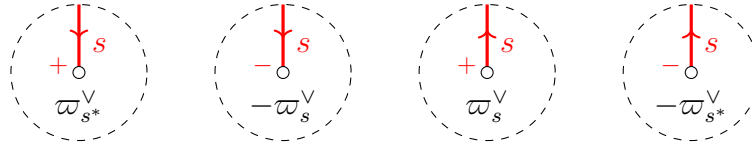


FIGURE 20. Contribution to $\theta_p(\widehat{L})$ from each end incident to the puncture p .

In general, the shear coordinates of W should be the same as the g -vector of the ‘pointed’ element F_W (cf. [Qin21]). In particular, the shear coordinates of the \mathfrak{g} -webs shown in Figure 21 are readily determined by this requirement (as they correspond to cluster variables):

$$F_W = \prod_{i \in I} A_i^{\tilde{x}_i(W)},$$

where we choose the cluster chart containing the cluster variable F_W ⁴. For example, the web W_s^E has exactly one +1 shear coordinate at the vertex on the edge E labeled by

⁴Here we should slightly modify the shear coordinates on the boundary to be the ‘Langlands dual’ version: see [IK22, Section 5].

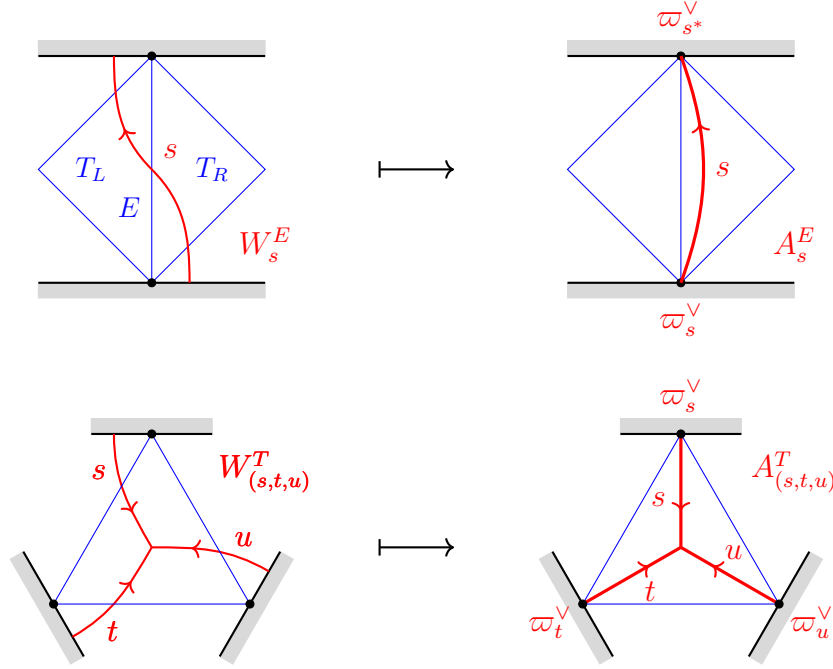


FIGURE 21. Some of the ‘elementary’ \mathfrak{g} -webs (Left) and the corresponding cluster variables on $\mathcal{A}_{G^\vee, \Sigma}$ with \mathfrak{g}^\vee -weights (Right). When some of the marked points are punctures and the signs of webs are $+$, the correspondence is still the same.

$s \in S$, while the others are 0. Observe that the assignment of the (co-)weights and the web description of cluster variables are consistent with the works [GS19, IY23, IY22].

Finally, the Weyl group action on the unbounded \mathfrak{g} -laminations should be defined so that the tropicalized Casimir map is equivariant with respect to the natural action on the coweight lattice. This requirement determines the action on a single signed end similarly to Definition 5.7. However, the check for the global consistency will require a hard elaboration as in Section 5.

We remark that in the case where $\mathfrak{g} = \mathfrak{sl}_3$, the intersection pairing between the bounded \mathfrak{sl}_3 -webs and certain unbounded \mathfrak{sl}_3 -webs is studied by Shen–Sun–Weng [SSW23]. It should be the same as the tropicalization of the quantum duality map. Intersection coordinates of bounded \mathfrak{sp}_4 -webs will be studied in the work of Ishibashi–Sun–Yuasa [ISY]. The higher rank version of shear coordinates for a general \mathfrak{g} -web should be defined so that the compatibility relation [IK22, Proposition 4.10] holds with these intersection coordinates.

APPENDIX A. CLUSTER VARIETIES ASSOCIATED WITH THE PAIR $(\mathfrak{sl}_3, \Sigma)$

Here we briefly recall the general theory of cluster varieties [FG09], and the construction of the seed pattern $\mathbf{s}(\mathfrak{sl}_3, \Sigma)$ that encodes the cluster structures of the spaces of \mathfrak{sl}_3 -laminations in consideration.

A.1. Cluster varieties. Fix a finite set $I = \{1, \dots, N\}$ of indices, and let \mathcal{F}_A and \mathcal{F}_X be fields both isomorphic to the field $\mathbb{Q}(z_1, \dots, z_N)$ of rational functions on N variables. We also fix a subset $I_{\text{uf}} \subset I$ (“unfrozen”) and let $I_f := I \setminus I_{\text{uf}}$ (“frozen”). Recall that a (*labeled, skew-symmetric*) *seed* in $(\mathcal{F}_A, \mathcal{F}_X)$ is a triple $(\varepsilon, \mathbf{A}, \mathbf{X})$, where

- $\varepsilon = (\varepsilon_{ij})_{i,j \in I}$ is a skew-symmetric matrix (*exchange matrix*) with values in $\frac{1}{2}\mathbb{Z}$ such that $\varepsilon_{ij} \in \mathbb{Z}$ unless $(i, j) \in I_f \times I_f$.
- $\mathbf{A} = (A_i)_{i \in I}$ and $\mathbf{X} = (X_i)_{i \in I}$ are tuples of algebraically independent elements (*cluster \mathcal{A} - and \mathcal{X} -variables*) in \mathcal{F}_A and \mathcal{F}_X , respectively.

We say that two seeds in $(\mathcal{F}_A, \mathcal{F}_X)$ are *mutation-equivalent* if they are transformed to each other by a finite sequence of mutations and permutations. The equivalence class is called a *mutation class*. Given a mutation class \mathbf{s} of seeds, we get:

The labeled exchange graph: a graph $\mathbb{E}\text{ch}_{\mathbf{s}}$ that parametrizes the seeds in \mathbf{s} .

When no confusion can occur, we simply denote its vertices by $v \in \mathbb{E}\text{ch}_{\mathbf{s}}$ instead of $v \in V(\mathbb{E}\text{ch}_{\mathbf{s}})$. For $v \in V(\mathbb{E}\text{ch}_{\mathbf{s}})$, we denote by $\mathbf{s}^{(v)} = (\varepsilon^{(v)}, \mathbf{A}^{(v)}, \mathbf{X}^{(v)})$ the corresponding seed.

The cluster varieties: schemes

$$\mathcal{X}_{\mathbf{s}} := \bigcup_{v \in \mathbb{E}\text{ch}_{\mathbf{s}}} \mathcal{X}_{(v)}, \quad \mathcal{A}_{\mathbf{s}} := \bigcup_{v \in \mathbb{E}\text{ch}_{\mathbf{s}}} \mathcal{A}_{(v)}.$$

Here $\mathcal{X}_{(v)} := \mathbb{T}_{N^{(v)}}$ and $\mathcal{A}_{(v)} := \mathbb{T}_{M^{(v)}}$; $N^{(v)} = \bigoplus_{i \in I} \mathbb{Z}e_i^{(v)}$ and $M^{(v)} = \bigoplus_{i \in I} \mathbb{Z}f_i^{(v)}$ are lattices dual to each other and $T_{\Lambda} := \text{Hom}(\Lambda^*, \mathbb{G}_m)$ denotes the algebraic torus corresponding to a lattice Λ . The tori $\mathcal{X}_{(v)}$, $v \in \mathbb{E}\text{ch}_{\mathbf{s}}$ are patched together according to the cluster \mathcal{X} -transformations, and similarly for the \mathcal{A} -side. We also have the cluster variety $\mathcal{X}_{\mathbf{s}}^{\text{uf}} := \bigcup_{v \in \mathbb{E}\text{ch}_{\mathbf{s}}} \mathcal{X}_{(v)}^{\text{uf}}$ without frozen coordinates. Here $\mathcal{X}_{(v)}^{\text{uf}} := \mathbb{T}_{N_{\text{uf}}^{(v)}}$ and $N_{\text{uf}}^{(v)} \subset N^{(v)}$ is the sub-lattice spanned by $e_i^{(v)}$ for $i \in I_{\text{uf}}$.

The ensemble map: a morphism $p : \mathcal{A}_{\mathbf{s}} \rightarrow \mathcal{X}_{\mathbf{s}}^{\text{uf}}$ given by the linear map

$$p_{(v)}^* : N_{\text{uf}}^{(v)} \rightarrow M^{(v)}, \quad e_i^{(v)} \mapsto \sum_{j \in I} \varepsilon_{ij}^{(v)} f_j^{(v)} \quad (\text{A.1})$$

on each torus at $v \in \mathbb{E}\text{ch}_{\mathbf{s}}$.

The cluster modular group: a subgroup $\Gamma_{\mathbf{s}} \subset \text{Aut}(\mathbb{E}\text{ch}_{\mathbf{s}})$ consisting of graph automorphisms ϕ which preserve the exchange matrices $\varepsilon^{(v)}$ assigned to vertices and the labels on the edges. The cluster modular group acts on the cluster varieties $\mathcal{A}_{\mathbf{s}}$ and $\mathcal{X}_{\mathbf{s}}$ so that $\phi^* Z_i^{(v)} = Z_i^{(\phi^{-1}(v))}$ for all $\phi \in \Gamma_{\mathbf{s}}$, $v \in \mathbb{E}\text{ch}_{\mathbf{s}}$ and $i \in I$, where $(Z, \mathcal{Z}) \in \{(A, \mathcal{A}), (X, \mathcal{X})\}$. These actions commute with the ensemble map.

The triple $(\mathcal{A}_{\mathbf{s}}, \mathcal{X}_{\mathbf{s}}^{\text{uf}}, p)$ is called a *cluster ensemble*. In this paper, we skip the discussion on the relation between $\mathcal{A}_{\mathbf{s}}$ and $\mathcal{X}_{\mathbf{s}}$. See [IK22, Appendix A] for a detail.

Cluster exact sequence. For $v, v' \in \mathbb{E}xch_s$, there are canonical identifications $\ker p_{(v)}^* \cong \ker p_{(v')}^*$ and $\operatorname{coker} p_{(v)}^* \cong \operatorname{coker} p_{(v')}^*$ given by the seed mutations in the sense of Fock–Goncharov [FG09, (7),(8)] and permutations. Under these identifications, let

$$K := \ker p_{(v)}^*, \quad K^\vee := (\operatorname{coker} p_{(v)}^*)^*,$$

and $H_{\mathcal{X}} := \mathbb{T}_K$, $H_{\mathcal{A}} := \mathbb{T}_{(K^\vee)^*} (= \mathbb{T}_{\operatorname{coker} p_{(v)}^*})$. The short exact sequences for the maps (A.1) commute with the cluster transformations by [FG09, Lemmas 2.7 and 2.10], and thus combine to give the following *cluster exact sequence*:

$$1 \rightarrow H_{\mathcal{A}} \rightarrow \mathcal{A}_s \xrightarrow{p} \mathcal{X}_s^{\text{uf}} \xrightarrow{\theta} H_{\mathcal{X}} \rightarrow 1, \quad (\text{A.2})$$

by which we mean that the ensemble map p is a principal $H_{\mathcal{A}}$ -bundle over its image, and the image coincides with the fiber $\theta^{-1}(1)$ of the map $\theta : \mathcal{X}_s \rightarrow H_{\mathcal{X}}$ induced by the inclusion $K \rightarrow N_{\text{uf}}^{(v)}$. By taking the character lattice X^* , we recover the exact sequence of (A.1) and by taking the cocharacter lattice X_* , we get its dual:

$$\begin{aligned} X^*(\text{A.2}) : \quad & 0 \leftarrow (K^\vee)^* \leftarrow M^{(v)} \xleftarrow{p^*} N_{\text{uf}}^{(v)} \leftarrow K \leftarrow 0, \\ X_*(\text{A.2}) : \quad & 0 \rightarrow K^\vee \rightarrow N^{(v)} \xrightarrow{(p^*)^\top} M_{\text{uf}}^{(v)} \rightarrow K^* \rightarrow 0. \end{aligned}$$

The sub-scheme $\mathcal{U}_s^{\text{uf}} := \theta^{-1}(1) = p(\mathcal{A}_s)$ is a symplectic leaf for the canonical Poisson structure determined by the exchange matrices. The cluster modular group also acts on the tori $H_{\mathcal{X}}$, $H_{\mathcal{A}}$ by monomial automorphisms, making the cluster exact sequence (A.2) Γ_s -equivariant.

An explicit description of the action of $H_{\mathcal{A}}$ on \mathcal{A}_s is as follows ([FG09, Section 2.3]). On the level of cocharacter lattices, it is just given by the additive action $K^\vee \otimes N^{(v)} \rightarrow N^{(v)}$. Given an element $\beta = \sum_i \beta_i^{(v)} e_i^{(v)} \in K^\vee$, let $\mathbb{G}_m \rightarrow H_{\mathcal{A}}$, $t \mapsto \beta(t)$ be the corresponding one-parameter subgroup. Then the action $\beta(t) : \mathcal{A}_{(v)} \rightarrow \mathcal{A}_{(v)}$ is written in terms of the cluster coordinates as

$$\beta(t)^* A_i^{(v)} = t^{\beta_i^{(v)}} A_i^{(v)}, \quad t \in \mathbb{G}_m. \quad (\text{A.3})$$

Tropicalizations. The positive structures on the cluster varieties allow us to consider their semifield-valued points. For $\mathbb{A} = \mathbb{Z}, \mathbb{Q}$ or \mathbb{R} , let $\mathbb{A}^T := (\mathbb{A}, \max, +)$ denote the corresponding *tropical semifield* (or the *max-plus semifield*). For an algebraic torus H , let $H(\mathbb{A}^T) := X_*(H) \otimes_{\mathbb{Z}} (\mathbb{A}, +)$. A positive rational map $f : H \rightarrow H'$ between algebraic tori naturally induces a piecewise-linear (PL for short) map $f^T : H(\mathbb{A}^T) \rightarrow H'(\mathbb{A}^T)$. We call f^T the *tropicalized map*. In particular we have the tropicalized cluster transformations $\mu_k^T : \mathcal{Z}_{(v)}(\mathbb{A}^T) \rightarrow \mathcal{Z}_{(v')}(\mathbb{A}^T)$ for $(z, \mathcal{Z}) \in \{(\mathbf{a}, \mathcal{A}), (\mathbf{x}, \mathcal{X})\}$, explicitly given as:

$$(\mu_k^T)^* \mathbf{x}_i^{(v')} = \begin{cases} -\mathbf{x}_k^{(v)} & \text{if } i = k, \\ \mathbf{x}_i^{(v)} - \varepsilon_{ik}^{(v)} [-\operatorname{sgn}(\varepsilon_{ik}^{(v)}) \mathbf{x}_k^{(v)}]_+ & \text{if } i \neq k, \end{cases} \quad (\text{A.4})$$

$$(\mu_k^T)^* \mathbf{a}_i^{(v')} = \begin{cases} -\mathbf{a}_k^{(v)} + \max \left\{ \sum_{j \in I} [\varepsilon_{kj}^{(v)}]_+ \mathbf{a}_j^{(v)}, \sum_{j \in I} [-\varepsilon_{kj}^{(v)}]_+ \mathbf{a}_j^{(v)} \right\} & \text{if } i = k, \\ \mathbf{a}_i^{(v)} & \text{if } i \neq k. \end{cases} \quad (\text{A.5})$$

Here $\mathbf{x}_i^{(v)}$ and $\mathbf{a}_i^{(v)}$ are the coordinate functions induced by the basis vectors $e_i^{(v)}$ and $f_i^{(v)}$ respectively, and $[u]_+ := \max\{0, u\}$ for $u \in \mathbb{A}$. We can use them to define the *tropical cluster varieties*

$$\mathcal{X}_s(\mathbb{A}^T) := \bigcup_{v \in \text{Exch}_s} \mathcal{X}_{(v)}(\mathbb{A}^T), \quad \mathcal{A}_s(\mathbb{A}^T) := \bigcup_{v \in \text{Exch}_s} \mathcal{A}_{(v)}(\mathbb{A}^T),$$

which are naturally equipped with canonical PL structures. Since the PL maps are equivariant for the scaling action of $\mathbb{A}_{>0}$, the tropical cluster varieties inherit this $\mathbb{A}_{>0}$ -action. We also have the tropical \mathcal{X} -varieties $\mathcal{X}_s^{\text{uf}}(\mathbb{A}^T)$ without frozen coordinates.

Since the above mentioned structures only involve positive rational maps, they are naturally inherited by the tropical cluster varieties. Thus we have:

- the cluster exact sequence

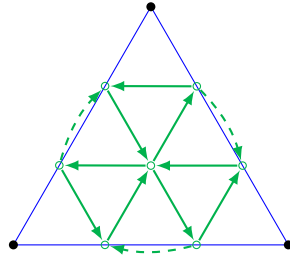
$$0 \rightarrow H_{\mathcal{A}}(\mathbb{A}^T) \rightarrow \mathcal{A}_s(\mathbb{A}^T) \xrightarrow{p} \mathcal{X}_s^{\text{uf}}(\mathbb{A}^T) \xrightarrow{\theta} H_{\mathcal{X}}(\mathbb{A}^T) \rightarrow 0 \quad (\text{A.6})$$

in the PL category, and

- the actions of Γ_s on $\mathcal{A}_s(\mathbb{A}^T)$ and $\mathcal{X}_s(\mathbb{A}^T)$ by PL automorphisms and on $H_{\mathcal{A}}(\mathbb{A}^T)$ and $H_{\mathcal{X}}(\mathbb{A}^T)$ by linear automorphisms, which make the cluster exact sequence Γ_s -equivariant. Moreover, these actions commute with the rescaling action of $\mathbb{A}_{>0}$.

A.2. The cluster ensemble associated with the pair $(\mathfrak{sl}_3, \Sigma)$. Here we quickly recall the cluster structures on the moduli spaces $\mathcal{A}_{SL_3, \Sigma}$ and $\mathcal{X}_{PGL_3, \Sigma}$ constructed in [FG06a]. We are going to recall the *Fock–Goncharov atlas* associated with ideal triangulations of Σ and their mutation-equivalences, since it is typically difficult to describe the entire cluster structure.

Let Δ be an ideal triangulation of Σ . Then we construct a quiver Q_{Δ} with the vertex set $I(\Delta)$ by drawing the quiver



on each triangle, and glue them by the *amalgamation* construction [FG06b]. In our case, this just means that we glue the quivers on adjacent triangles by identifying the two vertices on the shared edge and eliminating the pair of opposite dashed arrows. The vertices on the boundary intervals of Σ are declared to be frozen, forming the subset

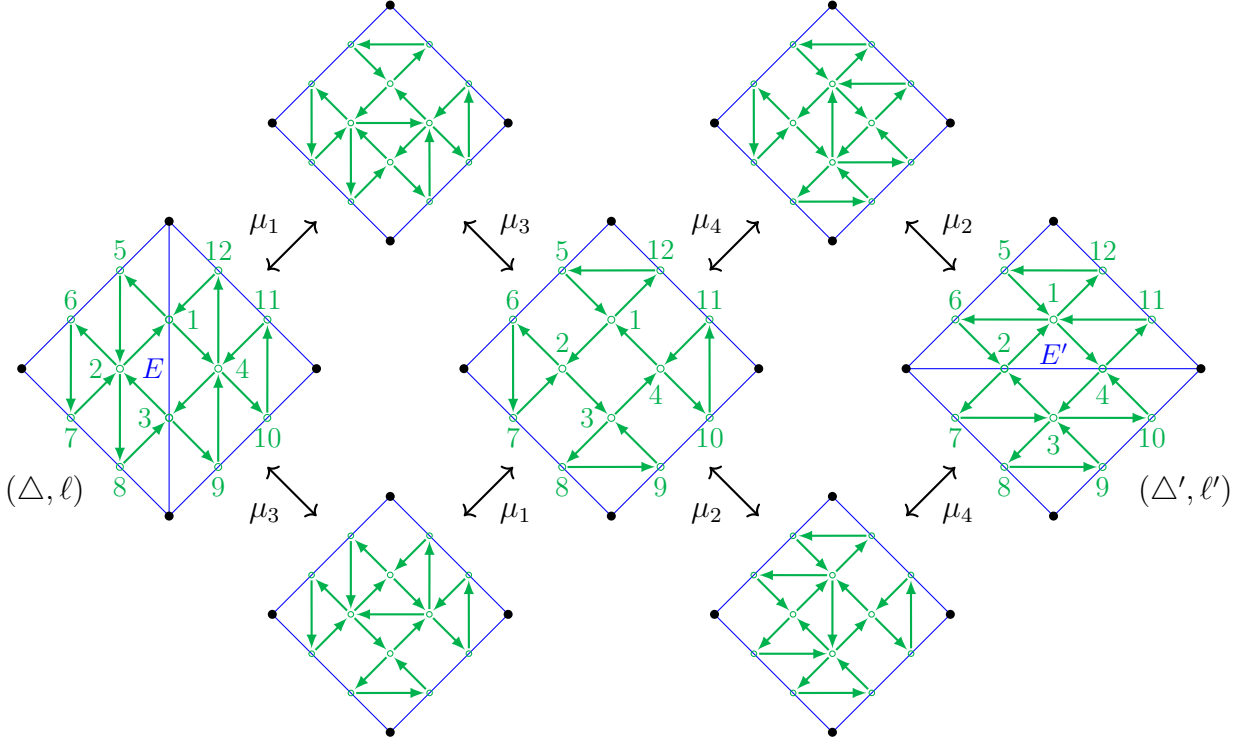


FIGURE 22. Some of the sequences of mutations that realize the flip $f_E : \Delta \rightarrow \Delta'$. Here we partially fix labelings ℓ, ℓ' of vertices in $I(\Delta), I(\Delta')$, respectively.

$I_f(\Delta) \subset I(\Delta)$ as in Section 2.1. Let $\varepsilon^\Delta = (\varepsilon_{ij}^\Delta)_{i,j \in I(\Delta)}$ be the corresponding exchange matrix.

These quivers Q^Δ (or the exchange matrices ε^Δ) associated with ideal triangulations of Σ are mutation-equivalent to each other. Indeed, the quivers $Q^\Delta, Q^{\Delta'}$ associated with two triangulations Δ, Δ' connected by a single flip $f_E : \Delta \rightarrow \Delta'$ are transformed to each other via one of the mutation sequences shown in Figure 22. Then the assertion follows from the classical fact that any two ideal triangulations of the same marked surface can be transformed to each other by a finite sequence of flips.

Then there exists a unique mutation class $\mathbf{s}(\mathfrak{sl}_3, \Sigma)$ containing the seeds associated with any ideal triangulations Δ . More precisely, a *labeled \mathfrak{sl}_3 -triangulation* (Δ, ℓ) , namely an ideal triangulation Δ together with a bijection $\ell : I(\Delta) \rightarrow \{1, \dots, N\}$, give rise to vertices of the labeled exchange graph $\mathbb{Exch}_{\mathbf{s}(\mathfrak{sl}_3, \Sigma)}$. Figure 22 describes a subgraph containing (Δ, ℓ) and (Δ', ℓ') , where the labels ℓ, ℓ' are consistently chosen. Let us simply denote the objects related to $\mathbf{s}(\mathfrak{sl}_3, \Sigma)$ by

$$\mathcal{A}_{\mathfrak{sl}_3, \Sigma} := \mathcal{A}_{\mathbf{s}(\mathfrak{sl}_3, \Sigma)}, \quad \mathcal{X}_{\mathfrak{sl}_3, \Sigma} := \mathcal{X}_{\mathbf{s}(\mathfrak{sl}_3, \Sigma)}, \quad \mathbb{Exch}_{\mathfrak{sl}_3, \Sigma} := \mathbb{Exch}_{\mathbf{s}(\mathfrak{sl}_3, \Sigma)}, \quad \Gamma_{\mathfrak{sl}_3, \Sigma} := \Gamma_{\mathbf{s}(\mathfrak{sl}_3, \Sigma)},$$

and so on.

Cluster modular group. Although the entire structure of the cluster modular group $\Gamma_{\mathfrak{sl}_3, \Sigma}$ is yet unknown, it is known to include the subgroup $(MC(\Sigma) \times \text{Out}(SL_3)) \ltimes W(\mathfrak{sl}_3)^{\mathbb{M}_o} \subset \Gamma_{\mathfrak{sl}_3, \Sigma}$ [GS18]. Here $MC(\Sigma)$ denotes the mapping class group of the marked surface Σ , $\text{Out}(SL_3) = \text{Aut}(SL_3)/\text{Inn}(SL_3)$ is the outer automorphism group of SL_3 , and $W(\mathfrak{sl}_3)$ is the Weyl group of the Lie algebra \mathfrak{sl}_3 . The group $\text{Out}(SL_3)$ has order 2, and generated by the *Dynkin involution* $* : G \rightarrow G, g \mapsto (g^{-1})^\top$.

Recall that the Weyl group $W(\mathfrak{sl}_3)$ is the group generated by two involutions r_1, r_2 , subject to the braid relation $r_1 r_2 r_1 = r_2 r_1 r_2$. The inclusion of $W(\mathfrak{sl}_3)^{\mathbb{M}_o}$ into the cluster modular group is given in [GS18, Section 8]. For simplicity, let us choose a labeled triangulation (Δ, ℓ) such that its local picture around p is as shown in Figure 23. Let $r_s^{(p)}$ denote the action of each generator assigned at p for $s = 1, 2$. Then the edge path $\gamma_s^{(p)}$ from (Δ, ℓ) to $r_s^{(p)} \cdot (\Delta, \ell)$ is described by the sequence

$$\mu_{\gamma_1^{(p)}} := \mu_3 \mu_4 \mu_5 (5 \ 6) \mu_5 \mu_4 \mu_3, \quad (\text{A.7})$$

$$\mu_{\gamma_2^{(p)}} := \mu_1 (1 \ 2) \mu_1. \quad (\text{A.8})$$

It turns out that the orders of mutations along the cycles $\{3, 4, 5, 6\}$ and $\{1, 2\}$ do not matter, and all define the same mutation loops [GS18, Theorem 7.1].

For each element ϕ in this subgroup, let us call the induced PL action $\phi : \mathcal{Z}_{\mathfrak{sl}_3, \Sigma}(\mathbb{Q}^T) \rightarrow \mathcal{Z}_{\mathfrak{sl}_3, \Sigma}(\mathbb{Q}^T)$ the *cluster action*, in comparison to the geometric action we introduce in the body of this paper in terms of signed \mathfrak{sl}_3 -webs.

Cluster exact sequence. We are going to investigate the tori $H_{\mathcal{X}}$ and $H_{\mathcal{A}}$ for the cluster ensemble associated with $\mathfrak{s}(\mathfrak{sl}_3, \Sigma)$.

For each puncture $p \in \mathbb{M}_o$, there exists an ideal triangulation $\Delta(p)$ of Σ such that the star neighborhood of p is a punctured disk with two marked points on its boundary. See, for instance, [HIO21, Lemma 5.7 (2)]. The corresponding quiver is shown in Figure 23, and we fix a labeling $\ell(p) : I(\Delta(p)) \rightarrow \{1, \dots, N\}$ as partially shown there. Then it can be easily seen from the quiver that the vectors

$$\begin{aligned} \alpha_1^{(p)} &:= e_3^{(v)} + e_4^{(v)} + e_5^{(v)} + e_6^{(v)}, \\ \alpha_2^{(p)} &:= e_1^{(v)} + e_2^{(v)} \end{aligned}$$

lie in $\ker p^* \subset N_{\text{uf}}^{(v)}$, where $v = (\Delta(p), \ell(p)) \in \mathbb{E}\text{ch}_{\mathfrak{sl}_3, \Sigma}$. The vectors $\alpha_s^{(p)}$ will behave as simple roots under the Weyl group actions (see below).

Lemma A.1 (cf. [GS19, Theorem 2.10 (2)]). *The set $\{\alpha_s^{(p)} \mid p \in \mathbb{M}_o, s = 1, 2\}$ is a \mathbb{Q} -basis of the vector space $X^*(H_{\mathcal{X}})_{\mathbb{Q}} = (\ker p^*)_{\mathbb{Q}}$. In particular, we have $H_{\mathcal{X}}(\mathbb{Q}^T) \cong \bigoplus_{p \in \mathbb{M}_o} \mathbb{P}_{\mathbb{Q}}^{\vee}$ by identifying the dual basis of $\alpha_s^{(p)}$ with the fundamental coweight $\varpi_s^{\vee} \in \mathbb{P}^{\vee}$.*

Indeed, the statement is verified by counting the dimensions of the relevant moduli spaces: see [FG06a, (2.10)]. The torus $H_{\mathcal{X}}$ covers the product $H^{\mathbb{M}_o}$ of copies of the Cartan subgroup $H' \subset PGL_3$. Via the birational isomorphism $\mathcal{X}_{\mathfrak{sl}_3, \Sigma}^{\text{uf}} \cong \mathcal{X}_{PGL_3, \Sigma}$ provided

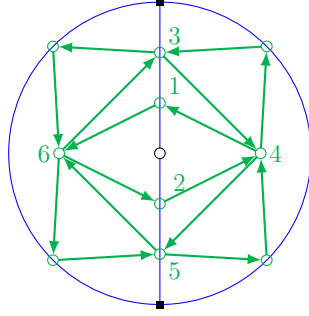


FIGURE 23. The quiver $Q^{\Delta(p)}$ around a puncture p . Here the possible (half-)arrows between boundary vertices are omitted.

by the cluster structure, each Cartan subgroup parametrizes the semisimple part of the monodromy around a puncture.

The torus $H_{\mathcal{A}}$ is described as follows. For each puncture p , choose $v = (\Delta(p), \ell(p))$ as above and consider

$$\begin{aligned} (\alpha_1^\vee)^{(p)} &:= e_3^{(v)} + e_4^{(v)} + e_5^{(v)} + e_6^{(v)}, \\ (\alpha_2^\vee)^{(p)} &:= e_1^{(v)} + e_2^{(v)}, \end{aligned}$$

which are now viewed as vectors in $K^\vee = (M^{(v)}/p^*(N_{\text{uf}}^{(v)}))^* \subset N^{(v)}$. For each special point $m \in M_\partial$, choose an ideal triangulation $\Delta(m)$ so that m belongs to a unique triangle, together with a labeling $\ell(m)$ as shown in Figure 24. Then the vectors

$$\begin{aligned} (\alpha_1^\vee)^{(m)} &:= e_3^{(v)} + e_4^{(v)} + e_5^{(v)}, \\ (\alpha_2^\vee)^{(m)} &:= e_1^{(v)} + e_2^{(v)} \end{aligned}$$

lie in K^\vee , where $v = (\Delta(m), \ell(m))$. The vectors $(\alpha_s^\vee)^{(m)}$ are viewed as simple coroots.

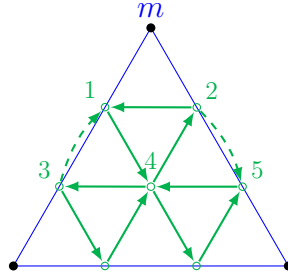


FIGURE 24. The quiver $Q^{\Delta(m)}$ around a special point m . Here possible (half-)arrows on the bottom edge are omitted.

Lemma A.2. *The set $\{(\alpha_s^\vee)^{(m)} \mid m \in \mathbb{M}, s = 1, 2\}$ is a \mathbb{Q} -basis of the vector space $X_*(H_{\mathcal{A}})_{\mathbb{Q}} = K_{\mathbb{Q}}^\vee$. In particular, we have $H_{\mathcal{A}}(\mathbb{Q}^T) \cong \bigoplus_{p \in \mathbb{M}_0} \mathbb{Q}_{\mathbb{Q}}^\vee$ by identifying the basis vector $(\alpha_s^\vee)^{(p)}$ with the simple coroot $\alpha_s^\vee \in \mathbb{Q}^\vee$.*

The statement is again verified by counting the dimension. The torus $H_{\mathcal{A}}$ covers the product $H^{\mathbb{M}}$ of copies of the Cartan subgroup $H \subset SL_3$. Via the birational isomorphism $\mathcal{A}_{\mathfrak{sl}_3, \Sigma} \cong \mathcal{A}_{SL_3, \Sigma}$ provided by the cluster structure, the action of each Cartan subgroup rescales the decoration assigned at a marked point.

The relations among the vector spaces are summarized as:

$$\begin{array}{ccc}
 & \bigoplus_{m \in \mathbb{M}} \mathbb{P}_{\mathbb{Q}} & \\
 X^*(\bullet)_{\mathbb{Q}} \swarrow & & \searrow X^*(\bullet)_{\mathbb{Q}} \\
 H_{\mathcal{A}} & & H_{\mathcal{X}} \\
 X_*(\bullet)_{\mathbb{Q}} \searrow & & \swarrow X_*(\bullet)_{\mathbb{Q}} \\
 & \bigoplus_{m \in \mathbb{M}} \mathbb{Q}_{\mathbb{Q}}^{\vee} & \\
 & \bigoplus_{p \in \mathbb{M}_o} \mathbb{Q}_{\mathbb{Q}} & \\
 & & \bigoplus_{p \in \mathbb{M}_o} \mathbb{P}_{\mathbb{Q}}^{\vee}
 \end{array}$$

In particular, we get the cluster exact sequence of the form

$$0 \rightarrow \bigoplus_{m \in \mathbb{M}} \mathbb{Q}_{\mathbb{Q}}^{\vee} \rightarrow \mathcal{A}_{\mathfrak{sl}_3, \Sigma}(\mathbb{Q}^T) \xrightarrow{p} \mathcal{X}_{\mathfrak{sl}_3, \Sigma}^{\text{uf}}(\mathbb{Q}^T) \xrightarrow{\theta} \bigoplus_{p \in \mathbb{M}_o} \mathbb{P}_{\mathbb{Q}}^{\vee} \rightarrow 0. \quad (\text{A.9})$$

APPENDIX B. LAMINATION CLUSTERS ALONG THE MUTATION SEQUENCE REPRESENTING $r_{p,s}$

We take the initial cluster as in Figure 23. Recall that the mutation sequences representing the actions $r_{p,2}$ and $r_{p,1}$ are given by

$$\mu_{\gamma_{p,2}} := (1 \ 2)\mu_2\mu_1, \quad \mu_{\gamma_{p,1}} := (5 \ 6)\mu_3\mu_4\mu_6\mu_5\mu_4\mu_3,$$

respectively. We show the lamination clusters along these mutation sequences in Figure 25 and Figure 26, respectively. Observe that the final cluster is indeed obtained from the initial one by applying the corresponding geometric actions together with the transpositions $(1 \ 2)$ and $(5 \ 6)$, respectively.

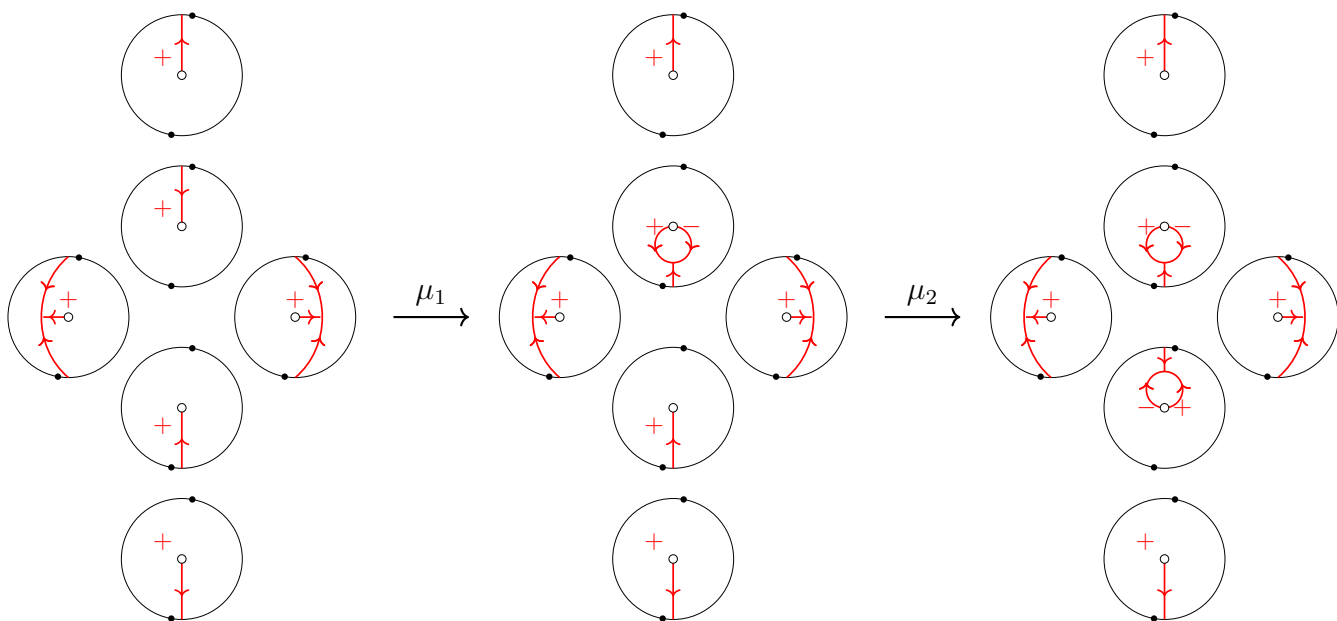


FIGURE 25. The sequence of lamination clusters along the mutation sequence for $r_{p,2}$.

REFERENCES

- [CKM14] S. Cautis, J. Kamnitzer, S. Morrison, *Webs and quantum skew Howe duality*, Math. Ann. **360** (2014), no. 1-2, 351–390. [4](#), [44](#)
- [DS20I] D. C. Douglas and Z. Sun, *Tropical Fock-Goncharov coordinates for SL_3 -webs on surfaces I: construction*, arXiv:2011.01768. [1](#), [9](#), [11](#), [13](#), [15](#)
- [DS20II] D. C. Douglas and Z. Sun, *Tropical Fock-Goncharov coordinates for SL_3 -webs on surfaces II: naturality*, arXiv:2012.14202. [11](#), [13](#)
- [FG06a] V. V. Fock and A. B. Goncharov, *Moduli spaces of local systems and higher Teichmüller theory*, Publ. Math. Inst. Hautes Études Sci., **103** (2006), 1–211. [4](#), [17](#), [50](#), [52](#)
- [FG06b] V. V. Fock and A. B. Goncharov, *Cluster \mathcal{X} -varieties, amalgamation and Poisson-Lie groups*, Algebraic geometry and number theory, volume 253 of Progr. Math., PP 27–68, Birkhäuser Boston, Boston, MA, 2006. [50](#)
- [FG07b] V. V. Fock and A. B. Goncharov, *Moduli spaces of convex projective structures on surfaces*, Adv. Math. **208** (2007), no. 1, 249–273. [4](#)
- [FG09] V. V. Fock and A. B. Goncharov, *Cluster ensembles, quantization and the dilogarithm*, Ann. Sci. Éc. Norm. Supér., **42** (2009), 865–930. [2](#), [3](#), [5](#), [7](#), [19](#), [45](#), [47](#), [49](#)
- [FP14] S. Fomin and P. Pylyavskyy, *Webs on surfaces, rings of invariants, and clusters*, Proc. Natl. Acad. Sci. USA **111** (2014), 9680–9687. [43](#)
- [FP16] S. Fomin and P. Pylyavskyy, *Tensor diagrams and cluster algebras*, Adv. Math. **300** (2016), 717–787. [43](#)
- [FP21] C. Fraser and P. Pylyavskyy, *Tensor diagrams and cluster combinatorics at punctures*, arXiv:2107.13069. [1](#), [4](#), [39](#), [40](#), [42](#), [43](#), [44](#)
- [FST08] S. Fomin, M. Shapiro and D. Thurston, *Cluster algebras and triangulated surfaces. I. Cluster complexes*, Acta Math. **201** (2008), 83–146. [2](#), [6](#), [42](#)

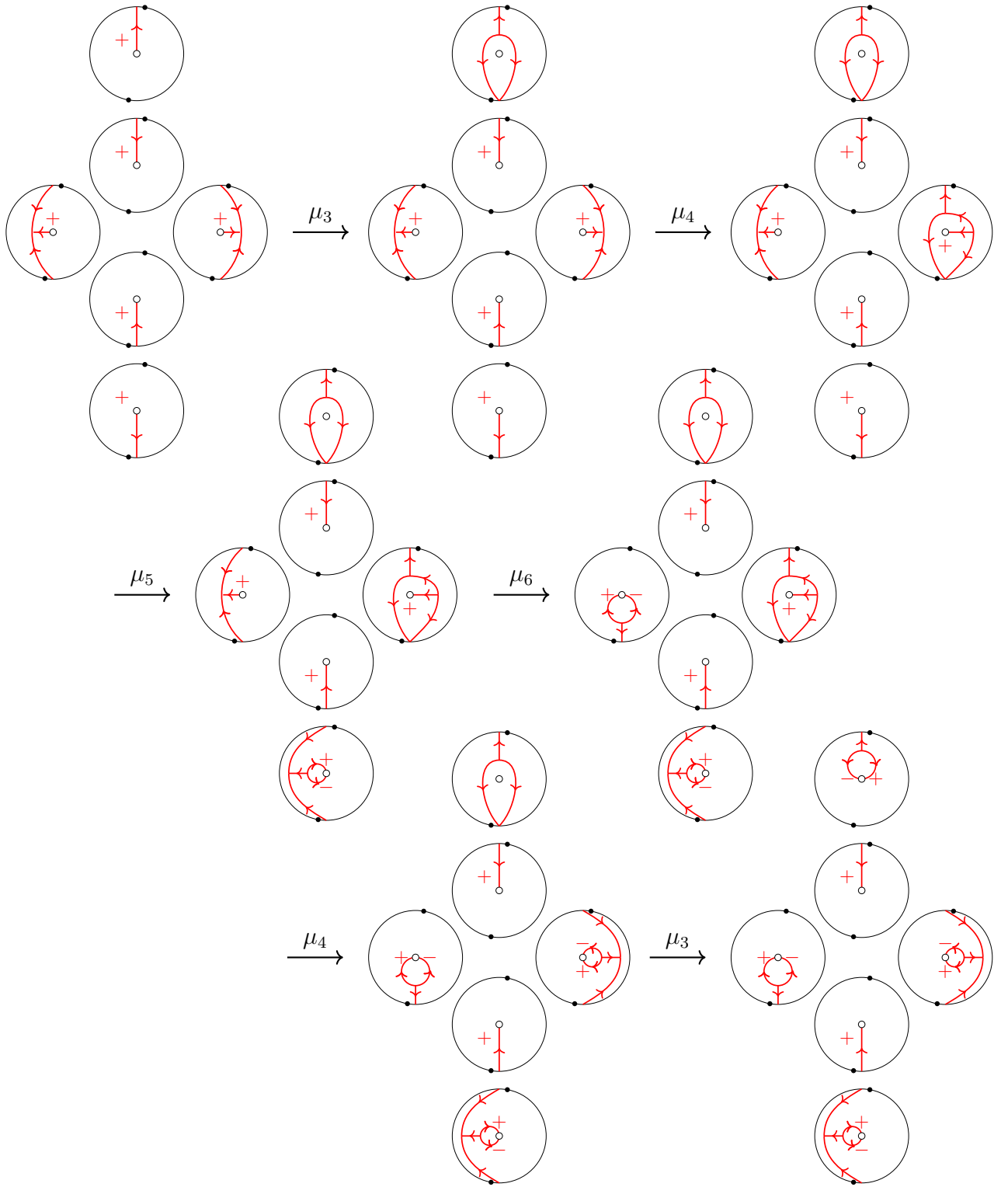


FIGURE 26. The sequence of lamination clusters along the mutation sequence for $r_{p,1}$.

- [FS20] C. Frohman and A. S. Sikora, *SU(3)-skein algebras and webs on surfaces*, Math. Z. **300** (2022), no. 1, 33–56. [9](#), [13](#), [15](#)
- [GS15] A. B. Goncharov and L. Shen, *Geometry of canonical bases and mirror symmetry*, Invent. Math. **202** (2015), no. 2, 487–633. [30](#)
- [GS18] A. B. Goncharov and L. Shen, *Donaldson-Thomas transformations of moduli spaces of G-local systems*, Adv. Math. **327** (2018), 225–348. [2](#), [3](#), [29](#), [30](#), [31](#), [52](#)
- [GS19] A. B. Goncharov and L. Shen, *Quantum geometry of moduli spaces of local systems and representation theory*, arXiv:1904.10491v3. [4](#), [30](#), [45](#), [47](#), [52](#)
- [IK22] T. Ishibashi and S. Kano, *Unbounded \mathfrak{sl}_3 -laminations and their shear coordinates*, arXiv:2204.08947; to appear in Algebr. Geom. Topol. **1**, [3](#), [4](#), [8](#), [9](#), [10](#), [11](#), [13](#), [14](#), [17](#), [21](#), [23](#), [24](#), [30](#), [31](#), [35](#), [36](#), [37](#), [38](#), [39](#), [45](#), [46](#), [47](#), [48](#)
- [IK23] T. Ishibashi and H. Karuo, *Quantum duality maps, skein algebras and their ensemble compatibility*, arXiv:2305.19074. [45](#)
- [IIO21] R. Inoue, T. Ishibashi and H. Oya, *Cluster realizations of Weyl groups and higher Teichmüller theory*, Sel. Math. New Ser. **27**, 37 (2021). [52](#)
- [IOS23] T. Ishibashi, H. Oya and L. Shen, *$\mathcal{A} = \mathcal{U}$ for cluster algebras from moduli spaces of G-local systems*, Adv. Math. **431** (2023). [4](#)
- [ISY] T. Ishibashi, Z. Sun and W. Yuasa, *Bounded \mathfrak{sp}_4 -laminations and their intersection coordinates*, in preparation. [47](#)
- [IY23] T. Ishibashi and W. Yuasa, *Skein and cluster algebras of unpunctured surfaces for \mathfrak{sl}_3* , Math. Z. **303**, 72 (2023). [47](#)
- [IY22] T. Ishibashi and W. Yuasa, *Skein and cluster algebras of unpunctured surfaces for \mathfrak{sp}_4* , arXiv:2207.01540. [47](#)
- [Kim21] H. K. Kim, *SL_3 -laminations as bases for PGL_3 cluster varieties for surfaces*, arXiv:2011.14765; to appear in Mem. Am. Math. Soc. **1**, [11](#), [44](#)
- [Kup96] G. Kuperberg, *Spiders for rank 2 Lie groups*, Comm. Math. Phys. **180** (1996), no. 1, 109–151. [1](#)
- [MOY98] H. Murakami, T. Ohtsuki and S. Yamada, *Homfly polynomial via an invariant of colored plane graphs*, Enseign. Math. (2) **44** (1998), no. 3-4, 325–360. [4](#), [44](#)
- [Qin21] F. Qin, *Cluster algebras and their bases*, arXiv:2108.09279. [46](#)
- [RY14] J. Roger and T. Yang, *The skein algebra of arcs and links and the decorated Teichmüller space*, J. Differential Geom. **96** (2014), no. 1, 95–140. [42](#)
- [SSW23] L. Shen, Z. Sun and D. Weng, *Intersections of Dual SL_3 -Webs*, arXiv:2311.15466. [1](#), [3](#), [4](#), [35](#), [36](#), [37](#), [47](#)
- [SSW] L. Shen, Z. Sun and D. Weng, *The punctured SL_3 skein algebra and the quantization of $\mathcal{A}_{SL_3, \hat{S}}$ moduli space*, in preparation. [42](#)

TSUKASA ISHIBASHI, MATHEMATICAL INSTITUTE, TOHOKU UNIVERSITY, 6-3 AOBA, ARAMAKI, AOBA-KU, SENDAI, MIYAGI 980-8578, JAPAN.

Email address: `tsukasa.ishibashi.a6@tohoku.ac.jp`

SHUNSUKE KANO, MATHEMATICAL SCIENCE CENTER FOR CO-CREATIVE SOCIETY, TOHOKU UNIVERSITY, 6-3 AOBA, ARAMAKI, AOBA-KU, SENDAI, MIYAGI 980-8578, JAPAN.

Email address: `s.kano@tohoku.ac.jp`